

Article

Further Optimization of Maxwell-Type Dynamic Vibration Absorber with Inerter and Negative Stiffness Spring Using Particle Swarm Algorithm

Yuying Chen ¹, Jing Li ^{1,*} , Shaotao Zhu ^{1,2,*} and Hongzhen Zhao ¹¹ Interdisciplinary Research Institute, Faculty of Science, Beijing University of Technology, Beijing 100124, China² Faculty of Information Technology, Beijing University of Technology, Beijing 100124, China

* Correspondence: leejing@bjut.edu.cn (J.L.); zhushaotao@bjut.edu.cn (S.Z.)

Abstract: Dynamic vibration absorbers (DVAs) are widely used in engineering practice because of their good vibration control performance. Structural design or parameter optimization could improve its control efficiency. In this paper, the viscoelastic Maxwell-type DVA model with an inerter and multiple stiffness springs is investigated with the combination of the traditional theory and an intelligent algorithm. Firstly, the expressions and approximate optimal values of the system parameters are obtained using the fixed-point theory to deal with the H_∞ optimization problem, which can provide help with the range of parameters in the algorithm. Secondly, we innovatively introduce the particle swarm optimization (PSO) algorithm to prove that the algorithm could adjust the value of the approximate solution to minimize the maximum amplitude by analyzing and optimizing the single variable and four variables. Furthermore, the validity of the parameters is further verified by simulation between the numerical solution and the analytical solution using the fourth-order Runge–Kutta method. Finally, the DVA demonstrated in this paper is compared with typical DVAs under random excitation. The timing sequence and variances, as well as the decreased ratios of the displacements, show that the presented DVA has a more satisfactory control performance. The inerter and negative stiffness spring can indeed bring beneficial effects to the vibration absorber. Remarkably, the intelligent algorithm can make the resonance peaks equal in the parameter optimization of the vibration absorber, which is quite difficult to achieve with theoretical methods at present. The results may provide a theoretical and computational basis for the optimization design of DVA.

Keywords: particle swarm optimization algorithm; dynamic vibration absorber; Maxwell-type; inerter; negative stiffness

MSC: 37N99; 68W99



Citation: Chen, Y.; Li, J.; Zhu, S.; Zhao, H. Further Optimization of Maxwell-Type Dynamic Vibration Absorber with Inerter and Negative Stiffness Spring Using Particle Swarm Algorithm. *Mathematics* **2023**, *11*, 1904. <https://doi.org/10.3390/math11081904>

Academic Editor: Jian Dong

Received: 6 March 2023

Revised: 7 April 2023

Accepted: 14 April 2023

Published: 17 April 2023



Copyright: © 2023 by the authors. Licensee MDPI, Basel, Switzerland. This article is an open access article distributed under the terms and conditions of the Creative Commons Attribution (CC BY) license (<https://creativecommons.org/licenses/by/4.0/>).

1. Introduction

Dynamic vibration absorbers (DVAs), known as tuned mass dampers (TMDs), are widely utilized in mechanical equipment and building structures owing to their favorable vibration control performance. The fundamental principle is to reduce the vibration state when an exciting force response occurs in the frequency domain by choosing the forms and parameters of the DVA as well as the coupling relationship with the primary system. In 1909, Frahm first proposed the concept of DVA as a passive vibration control device. In 1928, Ormondroyd and Den Hartog [1] introduced the damping effect to obtain the classical Voigt-type DVA and set minimizing the maximum amplitude response as the optimization goal. Hahnkamm [2] and Brock [3] successively derived the optimum tuning ratio and optimum damping ratio of this model, the method of which is now called the fixed-point theory through the textbook written by Den Hartog [4]. Subsequently, the design of three-element type DVA was further improved by Asami and Nishihara [5] based on the superb properties of viscoelastic devices. In 2001, Ren [6] developed a grounded

damped DVA that significantly enhances the vibration control. Under identical parameter conditions, the optimized Asami model and Ren model perform with superior control performance to the Voigt-type DVA. These three traditional models provide an irreplaceable reference value for future scholars to improve and optimize DVA structures.

Before introducing Maxwell model, we first trace the air damper that has a history of more than 80-year. This kind of damper is proposed due to its benefits such as temperature independent, less maintenance, low cost, and no long-term change. Asami and Sekiguchi [7,8] further put forward the piston-cylinder type air damper that could be represented by the Voigt model. This means that the elements of spring and damping were set in parallel. However, this equivalent structure made both the spring and damping parameters change with the frequency and affect each other. Taking into account the connection between the damping and restoring force in the actual damper, Asami and Nishihara [5] optimized the prior model and designed Maxwell structure, in which the spring and damping were connected in series. Moreover, the addition of a second spring element positioned parallel to the air damper could drive the piston to recover, and together they constitute the three-element type DVA. For viscoelastic materials with both damping and stiffness properties, the mechanical model with the Maxwell structure exhibits better results under the same mass ratio, one that has the value of further research in this paper.

Numerous experts also consider how to select and adapt parameters to achieve the best reduction in structural vibration in DVA while designing the ideal structure. The H_∞ optimization, the H_2 optimization, and the stability maximization criterion [9,10] are three common optimization criteria. The H_∞ optimization used in this study is more intuitive and convenient in practical application. The principle is to minimize the maximum amplitude when harmonic excitation acts on the primary system. Once we determined the optimization objective, the fixed-point theory can be applied as an approximate way to solve the parameter problem of the system. In addition, a new method was also developed by Asami et al. [11,12] to address the precise solution of H_∞ optimization. Both approaches aid in further improving the vibration reduction capacity of DVA. The conclusion shows that the approximate optimal solution is quite close to the precise solution, which verifies the usefulness of the fixed-point theory in an engineering context. Considering the simple and convenient reasons, this paper chooses the fixed-point theory to deal with H_∞ optimization and adjusts the value of the approximate solution with an intelligent algorithm to achieve minimizing the maximum amplitude more efficiently.

In the structural design of the vibration absorber, we can achieve the effect of vibration reduction by adding components. Negative stiffness usually means that the displacement of the object is opposite to the direction of the external force. It is a characteristic that is different from the negative Poisson ratio. Springs with negative stiffness are less stable. However, the study discovered that better vibration control performance will play out, and the natural frequency will decrease if the system has both positive and negative stiffness springs. This combination not only plays a role in high flexibility and high deformability but also maintains optimal stability under certain parameter conditions [13–15]. A negative stiffness characteristic has been applied to the design of composite materials and seismic retrofitting [16]. To lower the amplitude of the primary system, Shen and Wang et al. [17,18] inserted negative stiffness into the vibration absorbers (Ren model, three-element model) and confirmed the effective control performance. In addition to the negative stiffness elements discussed above, there is another element that is receiving increasing attention. Smith [19] proposed the idea of an inerter and solved the problem of synthesis on mechanical networks in 2002. As a new type of structural control device with two independent and free endpoints, the inerter has been found to achieve good results in vibration reduction or isolation and applied to suspension support design and simulation quality [20,21]. Based on the classical theory, Barredo et al. [22,23] and Wang et al. [24,25] optimized the DVA with an inerter, proving that it could maximize the applicable frequency range in vibration control. Furthermore, adding an amplifying mechanism [26] or distributed arrangement [27,28]

also makes the structure of the vibration absorber able to be further optimized, which is worth discussing in future work.

The optimization of DVA/TMD parameters has been investigated in depth in different various research backgrounds. Zhang and Xu [29] developed the optimization approach of TMD parameters, blending nonlinear aeroelastic effects for speeding control. Wang et al. [30] proposed a quasi-zero-stiffness energy harvesting DVA and optimized the parameters with the perturbation method to suppress vibration. In this paper, a swarm intelligence algorithm is innovatively introduced to find the global optimal value by following the currently searched optimal value and then determining the actual optimal value of each parameter [31,32]. In 1995, Kennedy and Eberhart proposed particle swarm optimization (PSO) when studying the predation behavior of birds. The algorithm transforms the entire group from disorder to order in the solution space by utilizing the sharing of information among group individuals. Moreover, the two extreme values of individual optimal value and group optimal value are tracked and updated by calculating the fitness of each particle. The particle swarm can identify the best position in accordance with the iteration termination condition and output the optimal parameter values when the maximum number of iterations is set. The theoretical optimal value obtained by the fixed-point theory to deal with the H_∞ optimization problem directly determines the range of parameters. With the support of the particle swarm optimization algorithm, the effect of the equal resonance peak is further realized, and the maximum amplitude of the primary system is minimized. This cannot be directly achieved by only using the theoretical method for parameter optimization. Using the algorithm to further optimize on the basis of the fixed-point theory can fully demonstrate its advantages in data processing. In the existing research on a Maxwell-type DVA/TMD with an inerter and negative stiffness spring, the combination of intelligent algorithm and theoretical analysis to automatically adjust the parameter strategy is our motivation and novelty.

The organization of this paper is as follows. The basic DVA model is given and the expressions of the system parameters are obtained in Section 2. The PSO algorithm is introduced in detail, and the numerical simulation is carried out according to different situations in Section 3. The DVA studied in this paper is compared with typical DVAs in Section 4. Finally, conclusion and prospect are drawn in Section 5.

2. Dynamic Vibration Absorber Model and Basic Parameter Optimization

2.1. The Basic Model and the Amplitude Response

This paper investigates the viscoelastic Maxwell-type DVA with an inerter and multiple stiffness springs, as displayed in Figure 1. The DVA is connected to a primary system with a single degree of freedom. m_1 , m_2 , k_1 , and k_2 are the masses and linear stiffness coefficients of the primary system and DVA severally. k_3 and c describe the stiffness and damping coefficient of Maxwell structure. b is the inerter. k_4 is the stiffness coefficient of the grounded negative stiffness spring. F_0 and ω denote the amplitude and frequency of the exciting force. x_1 , x_2 , and x_3 express the displacement of the primary system, DVA, and the division point about spring and damping in Maxwell structure.

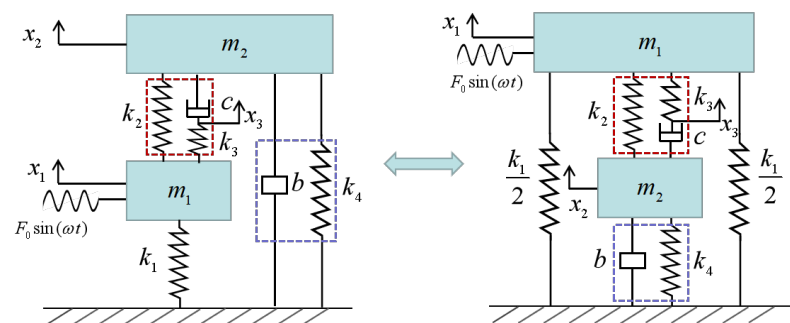


Figure 1. The viscoelastic Maxwell-type DVA with an inerter and multiple stiffness springs.

The dynamic equation of the system is established and obtained in accordance with Newton’s second law

$$\begin{cases} m_1\ddot{x}_1 + k_1x_1 + k_2(x_1 - x_2) + k_3(x_1 - x_3) = F_0 \sin(\omega t) \\ m_2\ddot{x}_2 + b\dot{x}_2 + c(\dot{x}_2 - \dot{x}_3) + k_2(x_2 - x_1) + k_4x_2 = 0 \\ c(\dot{x}_3 - \dot{x}_2) + k_3(x_3 - x_1) = 0 \end{cases} \tag{1}$$

By using the following parametric transformations

$$\omega_1 = \sqrt{\frac{k_1}{m_1}}, \omega_2 = \sqrt{\frac{k_2}{m_2}}, \zeta = \frac{c}{2m_2\omega_2}, \mu = \frac{m_2}{m_1}, \alpha_1 = \frac{k_3}{k_1}, \alpha_2 = \frac{k_4}{k_1}, \beta = \frac{b}{m_1}, f = \frac{F_0}{m_1}$$

Equation (1) can be expressed as

$$\begin{cases} \ddot{x}_1 + \omega_1^2x_1 + \mu\omega_2^2(x_1 - x_2) + \alpha_1\omega_1^2(x_1 - x_3) = f \sin(\omega t) \\ \ddot{x}_2 + \frac{\beta}{\mu}\ddot{x}_2 + 2\omega_2\zeta(\dot{x}_2 - \dot{x}_3) + \omega_2^2(x_2 - x_1) + \frac{\alpha_2\omega_1^2}{\mu}x_2 = 0 \\ 2\mu\omega_2\zeta(\dot{x}_3 - \dot{x}_2) + \alpha_1\omega_1^2(x_3 - x_1) = 0 \end{cases} \tag{2}$$

It should be noted that the representations of parameters $\alpha_1, \alpha_2, \beta$ are different from the existing literature [25]. Using this expressive method makes the process of theoretical derivation easier to implement in software. On the basis of Laplace transform, Equation (2) becomes

$$\begin{cases} (s^2 + \omega_1^2 + \mu\omega_2^2 + \alpha_1\omega_1^2)X_1(s) - \mu\omega_2^2X_2(s) - \alpha_1\omega_1^2X_3(s) = fe^{j\omega t} \\ -\omega_2^2X_1(s) + \left(s^2 + \frac{\beta}{\mu}s^2 + 2\omega_2\zeta s + \omega_2^2 + \frac{\alpha_2\omega_1^2}{\mu}\right)X_2(s) - 2\omega_2\zeta sX_3(s) = 0 \\ -\alpha_1\omega_1^2X_1(s) - 2\mu\omega_2\zeta sX_2(s) + (2\mu\omega_2\zeta s + \alpha_1\omega_1^2)X_3(s) = 0 \end{cases} \tag{3}$$

Supposing $X_1(s) = H_1(j\omega)e^{j\omega t}$, $X_2(s) = H_2(j\omega)e^{j\omega t}$, $X_3(s) = H_3(j\omega)e^{j\omega t}$ and letting $s = j\omega$, $j = \sqrt{-1}$, one could obtain by substituting them into Equation (3)

$$H_1(j\omega) = \frac{f(A_1 + B_1j)}{C_1 + D_1j}$$

The other parameters are presented as

$$\begin{aligned} A_1 &= \alpha_1\omega_1^2 [\alpha_2\omega_1^2 + \mu\omega_2^2 - (\mu + \beta)\omega^2] \\ B_1 &= 2\mu\omega\omega_2\zeta [(\alpha_1 + \alpha_2)\omega_1^2 + \mu\omega_2^2 - (\mu + \beta)\omega^2] \\ C_1 &= \alpha_1\omega_1^2 \{(\mu + \beta)\omega^4 - [(\alpha_2 + \mu + \beta)\omega_1^2 + \mu(1 + \mu + \beta)\omega_2^2] \omega^2 \\ &\quad + \mu(1 + \alpha_2)\omega_1^2\omega_2^2 + \alpha_2\omega_1^4\} \\ D_1 &= 2\mu\omega\omega_2\zeta \{(\mu + \beta)\omega^4 + \mu(1 + \alpha_2)\omega_1^2\omega_2^2 + (\alpha_1 + \alpha_2 + \alpha_1\alpha_2)\omega_1^4 \\ &\quad - \{[\alpha_1 + \alpha_2 + (\mu + \beta)(1 + \alpha_1)]\omega_1^2 + \mu(1 + \mu + \beta)\omega_2^2\} \omega^2\} \end{aligned}$$

Introducing the parameters

$$v = \frac{\omega_2}{\omega_1}, \lambda = \frac{\omega}{\omega_1}, X_{st} = \frac{F_0}{k_1}$$

where X_{st} is the static deformation of the primary system under sinusoidal excitation. The amplitude amplification factor should be

$$A^2 = \left| \frac{H_1}{X_{st}} \right|^2 = \frac{A_2^2 + \zeta^2 B_2^2}{C_2^2 + \zeta^2 D_2^2} \tag{4}$$

where

$$\begin{aligned}
 A_2 &= \alpha_1 [\alpha_2 + \mu v^2 - (\mu + \beta)\lambda^2] \\
 B_2 &= 2\mu\lambda v [\alpha_1 + \alpha_2 + \mu v^2 - (\mu + \beta)\lambda^2] \\
 C_2 &= \alpha_1 \{(\mu + \beta)\lambda^4 - [\alpha_2 + \mu + \beta + \mu(1 + \mu + \beta)v^2]\lambda^2 \\
 &\quad + \mu(1 + \alpha_2)v^2 + \alpha_2\} \\
 D_2 &= 2\mu\lambda v \{(\mu + \beta)\lambda^4 + \mu(1 + \alpha_2)v^2 + \alpha_1 + \alpha_2 + \alpha_1\alpha_2 \\
 &\quad - [\alpha_1 + \alpha_2 + (\mu + \beta)(1 + \alpha_1) + \mu(1 + \mu + \beta)v^2]\lambda^2\}
 \end{aligned}$$

2.2. The Optimum Frequency Ratio v_{opt} and the Optimum Stiffness Ratio α_{1opt}

It can be demonstrated after simple derivation of Equation (4) that the normalized amplitude–frequency curves pass through three fixed points of DVA, which are independent of the damping ratio ζ . Figure 2a provides the curves under different damping ratios of 0.3, 0.5, and 0.9. Three fixed points are represented here as $P, Q,$ and R . Other parameters are fixed as $\mu = 0.1, \beta = 0.3, v = 1.4, \alpha_1 = 0.3,$ and $\alpha_2 = -0.1$. Since the fixed points are independent of the damping ratio, it is necessary to make the response values of $\zeta \rightarrow 0$ and $\zeta \rightarrow \infty$ equal to solve its analytical expression, which satisfies the following equation

$$\left| \frac{A_2}{C_2} \right|_{\zeta \rightarrow 0} = \left| \frac{B_2}{D_2} \right|_{\zeta \rightarrow \infty} \tag{5}$$

One can obtain from simplification

$$g(\lambda) = a_1\lambda^6 + a_2\lambda^4 + a_3\lambda^2 + a_4 = 0 \tag{6}$$

where

$$\begin{aligned}
 a_1 &= -2(\mu + \beta)^2 \\
 a_2 &= 2v^2\mu^3 + [2 + \alpha_1 + 4(1 + \beta)v^2]\mu^2 + [2(\alpha_1 + 2\alpha_2) + \beta(2 + \alpha_1)]\beta \\
 &\quad + 2[\alpha_1(1 + \beta) + 2(\alpha_2 + \beta) + \beta(2 + \beta)v^2]\mu \\
 a_3 &= -\{2\mu^3v^4 + 2[2 + \alpha_1 + 2\alpha_2 + (1 + \beta)v^2]\mu^2v^2 \\
 &\quad + 2\{[\alpha_1(1 + \beta) + 2\alpha_2 + 2\beta(1 + \alpha_2)]v^2 + \alpha_1(1 + \alpha_2) + 2\alpha_2\}\mu \\
 &\quad + 2\beta[\alpha_1(1 + \alpha_2) + 2\alpha_2] + 2\alpha_2(\alpha_1 + \alpha_2)\} \\
 a_4 &= 2(1 + \alpha_2)\mu^2v^4 + 2\mu[\alpha_1(1 + \alpha_2) + \alpha_2(2 + \alpha_2)]v^2 + \alpha_1\alpha_2(2 + \alpha_2) + 2\alpha_2^2
 \end{aligned}$$

When $\zeta \rightarrow 0$, one has

$$|A| = \left| \frac{H_1}{X_{st}} \right| = \left| \frac{A_3}{C_3} \right| \tag{7}$$

When $\zeta \rightarrow \infty$, one has

$$|A| = \left| \frac{H_1}{X_{st}} \right| = \left| \frac{B_3}{D_3} \right| \tag{8}$$

where

$$A_3 = \frac{A_2}{\alpha_1}, B_3 = \frac{B_2}{2\mu\lambda v}, C_3 = \frac{C_2}{\alpha_1}, D_3 = \frac{D_2}{2\mu\lambda v}$$

Equations (7) and (8) are combined to determine the coordinates of three points:

$$|A| = \left| \frac{H_1}{X_{st}} \right| = \left| \frac{\alpha_1 + 2\alpha_2 + 2\mu v^2 - 2(\mu + \beta)\lambda^2}{\alpha_1[1 + \alpha_2 - (1 + \mu + \beta)\lambda^2]} \right| \tag{9}$$

Let λ_P^2 , λ_Q^2 , and λ_R^2 be the three roots of Equation (9). As long as the values of λ_P , λ_Q , and λ_R are determined, the coordinates of the three points can be written. The optimum frequency ratio, the optimum stiffness ratio, and the optimum damping ratio can be obtained when the vertical ordinates are adjusted to the same height, thereby solving the problem of minimizing the maximum amplitude. By drawing the normalized amplitude–frequency curves of $\zeta \rightarrow 0$ and $\zeta \rightarrow \infty$ as shown in Figure 2b, it is found that there is a fixed phase difference between two points P , R , and point Q . Therefore, there is a positive and negative sign difference when the absolute value is removed in Equation (9).

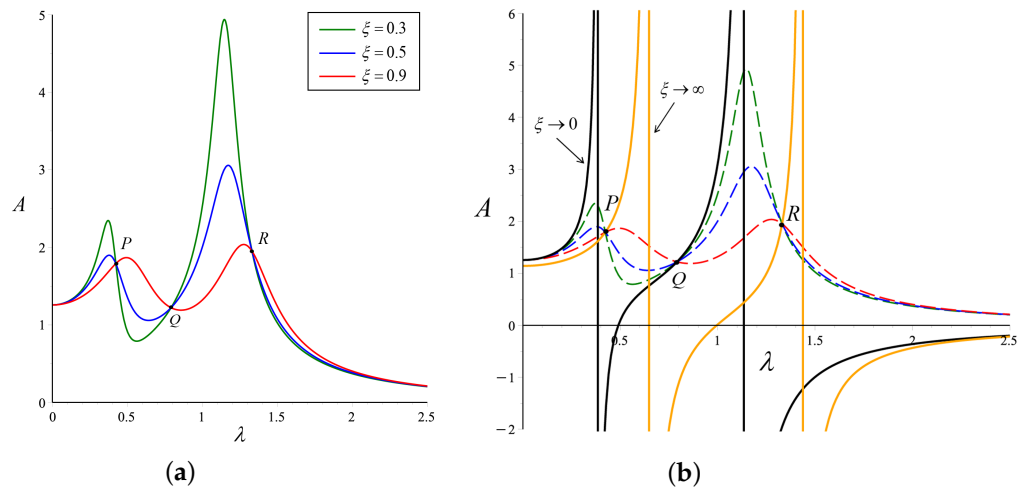


Figure 2. The normalized amplitude–frequency curves under different damping ratios: (a) $\zeta = 0.3$, $\zeta = 0.5$, and $\zeta = 0.9$; (b) $\zeta \rightarrow 0$ and $\zeta \rightarrow \infty$.

The first step is adjusting the ordinates of point P and point R to the equal height

$$\left| \frac{H_1}{X_{st}} \right|_P = \left| \frac{A_4 + B_4 \lambda_P^2}{C_4 + D_4 \lambda_P^2} \right|, \left| \frac{H_1}{X_{st}} \right|_R = \left| \frac{A_4 + B_4 \lambda_R^2}{C_4 + D_4 \lambda_R^2} \right| \tag{10}$$

where

$$A_4 = \alpha_1 + 2\alpha_2 + 2\mu v^2, \quad B_4 = -2(\mu + \beta)$$

$$C_4 = \alpha_1(1 + \alpha_2), \quad D_4 = -\alpha_1(1 + \mu + \beta)$$

When the parameter α_1 satisfies $A_4 D_4 = B_4 C_4$, the ordinates of two fixed points P and R are independent of λ^2 . One could gain

$$\alpha_1 = \frac{2[\mu + \beta - \alpha_2 - \mu(1 + \mu + \beta)v^2]}{1 + \mu + \beta} \tag{11}$$

Substituting α_1 into Equation (6), we can obtain

$$\frac{2}{1 + \mu + \beta} \left[(1 + \mu + \beta)\lambda^2 - (1 + \alpha_2) \right] \{ (\mu + \beta)^2 \lambda^4 - 2(\mu + \beta)^2 \lambda^2 - (1 + \mu + \beta)\mu^2 v^4 + 2(\mu + \beta - \alpha_2)\mu v^2 + \alpha_2[2(\mu + \beta) - \alpha_2] \} = 0 \tag{12}$$

The values of λ_P^2 , λ_Q^2 and λ_R^2 are obtained from Equation (12)

$$\lambda_P^2 = \frac{\mu + \beta - \sqrt{(1 + \mu + \beta)\mu^2 v^4 - 2(\mu + \beta - \alpha_2)\mu v^2 + (\mu + \beta - \alpha_2)^2}}{\mu + \beta} \tag{13a}$$

$$\lambda_Q^2 = \frac{1 + \alpha_2}{1 + \mu + \beta} \tag{13b}$$

$$\lambda_R^2 = \frac{\mu + \beta + \sqrt{(1 + \mu + \beta)\mu^2v^4 - 2(\mu + \beta - \alpha_2)\mu v^2 + (\mu + \beta - \alpha_2)^2}}{\mu + \beta} \tag{13c}$$

Then, Equation (9) becomes

$$\left| \frac{H_1}{X_{st}} \right|_{P,R} = \frac{\mu + \beta}{\mu + \beta - \alpha_2 - \mu(1 + \mu + \beta)v^2} \tag{14a}$$

$$\left| \frac{H_1}{X_{st}} \right|_Q = \frac{(1 + \mu + \beta)[\mu + \beta - \alpha_2 - \mu(1 + \mu + \beta)v^2]}{(\mu + \beta - \alpha_2)^2} \tag{14b}$$

The second step is adjusting the ordinates of point P (or R) and point Q to the same height. The optimum frequency ratio could be

$$v_{opt} = \sqrt{\frac{(1 + \mu + \beta)(\mu + \beta - \alpha_2) - \sqrt{(\mu + \beta)(\mu + \beta - \alpha_2)^2(1 + \mu + \beta)}}{\mu(1 + \mu + \beta)^2}} \tag{15}$$

Then, we can substitute Equation (15) into Equation (11) to obtain

$$\alpha_{1opt} = \frac{2\sqrt{(\mu + \beta)(\mu + \beta - \alpha_2)^2(1 + \mu + \beta)}}{(1 + \mu + \beta)^2} \tag{16}$$

and

$$\left| \frac{H_1}{X_{st}} \right|_{P,Q,R} = \sqrt{\frac{(\mu + \beta)(1 + \mu + \beta)}{(\mu + \beta - \alpha_2)^2}} \tag{17}$$

2.3. The Optimum Stiffness Ratio α_{2opt} and the Optimum Damping Ratio ζ_{opt}

Because the inappropriate stiffness value will make the system unstable, it is discovered that the system will be in a stable state when the displacement caused by the pre-load is equivalent to the response value at the fixed point.

$$\left| \frac{H_1}{X_{st}} \right|_{\lambda=0} = \left| \frac{H_1}{X_{st}} \right|_{P,Q,R} \tag{18}$$

that is,

$$\left| \frac{H_1}{X_{st}} \right|_{\lambda=0} = \frac{(1 + \mu + \beta)(\mu + \beta)(1 + \alpha_2) - M_1}{\alpha_2(1 + \mu + \beta)^2 + (1 + \alpha_2)\{ (1 + \mu + \beta)(\mu + \beta - \alpha_2) - M_1 \}} \tag{19}$$

where

$$M_1 = \sqrt{(\mu + \beta)(\mu + \beta - \alpha_2)^2(1 + \mu + \beta)}$$

Based on Equations (17) and (19), the stiffness ratio α_2 of system is shown as the following five possible forms

$$\alpha_{2a,2b} = \frac{\mu + \beta + 2(1 + \mu + \beta) \left[\mu + \beta \pm \sqrt{(\mu + \beta)(1 + \mu + \beta)} \right]}{3(1 + \mu + \beta) + 1} \tag{20a}$$

$$\alpha_{2c,2d} = \frac{\mu + \beta + (1 + \mu + \beta) \left[\mu + \beta \pm \sqrt{(\mu + \beta)(2 + \mu + \beta)} \right]}{2 + \mu + \beta} \tag{20b}$$

$$\alpha_{2e} = -1 \tag{20c}$$

The frequency of force excitation is obtained according to Equation (4)

$$\omega_{(1,2)}^2 = \frac{(\mu + \beta + \alpha_2)\omega_1^2 + \mu(1 + \mu + \beta)\omega_2^2 \pm \sqrt{\Delta}}{2(\mu + \beta)} \tag{21}$$

where

$$\Delta = \left[(\mu + \beta + \alpha_2)\omega_1^2 + \mu(1 + \mu + \beta)\omega_2^2 \right]^2 - 4(\mu + \beta) \left[\mu(1 + \alpha_2)\omega_1^2\omega_2^2 + \alpha_2\omega_1^4 \right]$$

When

$$\alpha_2 > -\frac{\mu\omega_2^2}{\omega_1^2 + \mu\omega_2^2} = \alpha_2 > -\frac{1}{1 + \frac{1}{\mu\nu^2}} > -1$$

the frequency of force excitation is nonnegative. From this condition, it can be determined that the value of α_2 should first exclude $\alpha_{2e} = -1$, and the other value relationship is shown in Figure 3. Furthermore, we substitute $\alpha_{2a} - \alpha_{2d}$ into ν and find that α_{2a} or α_{2c} makes ν purely imaginary. This loses the significance of variables optimizing the system, so α_{2b} and α_{2d} are the best values for now. In other words, the inerter-to-mass ratio can keep the system stable and reduce the vibration within the corresponding range when $\alpha_{opt} = \alpha_{2b}$ and $\alpha_{opt} = \alpha_{2d}$. We discuss the selection of the optimal parameters in the following two situations. The relationship between $(\mu, \beta, \nu(\alpha_2))$ and $(\mu, \beta, \alpha_1(\alpha_2))$ can be seen from Figures 4 and 5.

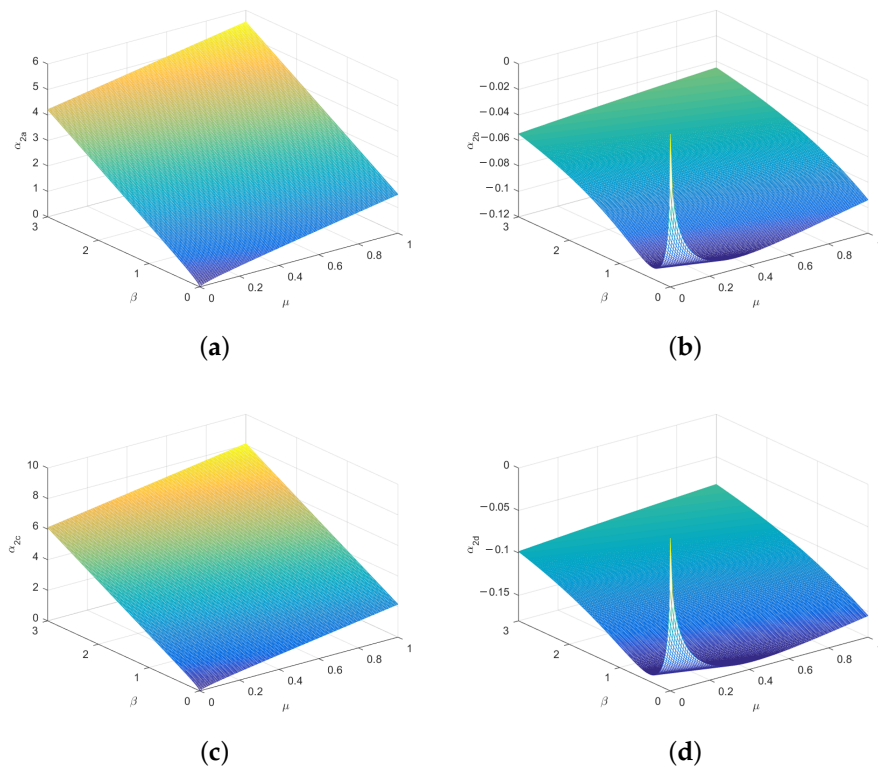


Figure 3. The relationship of (μ, β, α_2) : (a) $(\mu, \beta, \alpha_{2a})$ space; (b) $(\mu, \beta, \alpha_{2b})$ space; (c) $(\mu, \beta, \alpha_{2c})$ space; (d) $(\mu, \beta, \alpha_{2d})$ space.

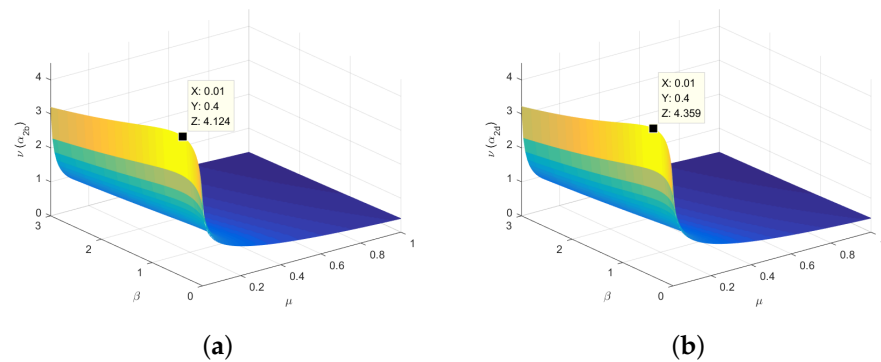


Figure 4. The relationship of $(\mu, \beta, \nu(\alpha_2))$: (a) $(\mu, \beta, \nu(\alpha_{2b}))$ space; (b) $(\mu, \beta, \nu(\alpha_{2d}))$ space.

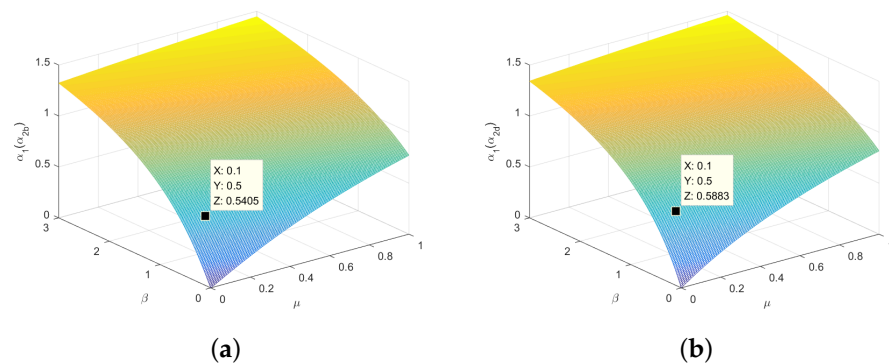


Figure 5. The relationship of $(\mu, \beta, \alpha_1(\alpha_2))$: (a) $(\mu, \beta, \alpha_1(\alpha_{2b}))$ space; (b) $(\mu, \beta, \alpha_1(\alpha_{2d}))$ space.

According to the fixed-point theory, any damping ratio change will go through three fixed points. When the three fixed points are adjusted to the same height, the two resonance peaks can be also maintained to be equal as possible by changing the damping ratio ζ . In order to obtain the optimum damping ratio, it is necessary to know the horizontal coordinates of two resonance peaks, namely λ_1 and λ_2 . It can be observed that when the two resonance peaks are almost at the same height, the vicinity of point Q is in the region where the slope of the amplitude-frequency curve is zero. According to the previous calculation results, the abscissa of point Q has been solved. The explicit expression can obtain the approximate optimum damping ratio based on the abscissa of point Q.

$$(1) \alpha_{2opt} = \alpha_{2b} \Rightarrow \begin{cases} \frac{\partial A^2}{\partial \lambda_Q^2} = 0 \\ \alpha_{1opt} = \frac{2\sqrt{(\mu+\beta)(\mu+\beta-\alpha_{2b})^2(1+\mu+\beta)}}{(1+\mu+\beta)^2} \\ \nu_{opt} = \sqrt{\frac{(1+\mu+\beta)(\mu+\beta-\alpha_{2b}) - \sqrt{(\mu+\beta)(\mu+\beta-\alpha_{2b})^2(1+\mu+\beta)}}{\mu(1+\mu+\beta)^2}} \\ \alpha_{2b} = \frac{\mu+\beta+2(1+\mu+\beta)[\mu+\beta-\sqrt{(\mu+\beta)(1+\mu+\beta)}]}{3(1+\mu+\beta)+1} \\ \lambda_Q^2 = \frac{1+\alpha_{2b}}{1+\mu+\beta} \end{cases}$$

$$(2) \alpha_{2opt} = \alpha_{2d} \Rightarrow \begin{cases} \frac{\partial A^2}{\partial \lambda_Q^2} = 0 \\ \alpha_{1opt} = \frac{2\sqrt{(\mu+\beta)(\mu+\beta-\alpha_{2d})^2(1+\mu+\beta)}}{(1+\mu+\beta)^2} \\ v_{opt} = \sqrt{\frac{(1+\mu+\beta)(\mu+\beta-\alpha_{2d}) - \sqrt{(\mu+\beta)(\mu+\beta-\alpha_{2d})^2(1+\mu+\beta)}}{\mu(1+\mu+\beta)^2}} \\ \alpha_{2d} = \frac{\mu+\beta+(1+\mu+\beta)\left[\mu+\beta-\sqrt{(\mu+\beta)(2+\mu+\beta)}\right]}{2+\mu+\beta} \\ \lambda_Q^2 = \frac{1+\alpha_{2d}}{1+\mu+\beta} \end{cases}$$

$$\begin{aligned} p_1 &= (A_2^2)' = 2\alpha_1^2(\mu + \beta) \left[(\mu + \beta)\lambda^2 - \alpha_2 - \mu v^2 \right] \\ p_2 &= (B_2^2)' = 4\mu^2 v^2 \left[3(\mu + \beta)^2 \lambda^4 - 4(\mu + \beta)M_2 \lambda^2 + M_2^2 \right] \\ q_1 &= (C_2^2)' = 2\alpha_1^2 \{ 2(\mu + \beta)^2 \lambda^6 - 3(\mu + \beta)M_3 \lambda^4 + [M_3^2 + 2(\mu + \beta)M_4] \lambda^2 - M_3 M_4 \} \\ q_2 &= (D_2^2)' = 4\mu^2 v^2 \{ 5(\mu + \beta)^2 \lambda^8 - 8(\mu + \beta)M_5 \lambda^6 + 3[M_5^2 + 2(\mu + \beta)M_6] \lambda^4 \\ &\quad - 4M_5 M_6 \lambda^2 + M_6^2 \} \end{aligned}$$

where

$$\begin{aligned} M_2 &= \alpha_1 + \alpha_2 + \mu v^2 \\ M_3 &= \alpha_2 + \mu + \beta + \mu(1 + \mu + \beta)v^2 \\ M_4 &= \alpha_2 + \mu(1 + \alpha_2)v^2 \\ M_5 &= \alpha_1 + \alpha_2 + (\mu + \beta)(1 + \alpha_1) + \mu(1 + \mu + \beta)v^2 \\ M_6 &= \alpha_1 + \alpha_2 + \alpha_1 \alpha_2 + \mu(1 + \alpha_2)v^2 \end{aligned}$$

Let $p = A_2^2 + \xi^2 B_2^2$ and $q = C_2^2 + \xi^2 D_2^2$

$$\frac{\partial A^2}{\partial \lambda_Q^2} = \left(\frac{p}{q} \right)' = \frac{p'q - pq'}{q^2} = 0 \Leftrightarrow (p_1 + \xi^2 p_2)' q - (q_1 + \xi^2 q_2)' p = 0 \Leftrightarrow \text{solve } \xi$$

In the previous analysis and calculation, we obtained the optimal-value expressions of some parameters related to μ and β . For the mass ratio μ related to the primary system and DVA, the final control results are ideal when μ is limited between 0.05 and 0.5. This is because the range of m_2 is not arbitrarily determined in the actual design of DVA, and it is usually necessary to consider the installation space, manufacturing cost, installation difficulty, and other factors. If m_2 is very small, the natural frequency will be too close to reduce the vibration control. If m_2 is too large, the practicability of the whole device will be greatly affected. Therefore, it is found in the literature that experts and scholars usually take the range of μ to optimize the design, so as to determine the optimal value.

We take $\alpha_{2opt} = \alpha_{2b}$ as an example to compare the numerical and analytical solutions for different mass ratios μ and different inerter-to-mass ratios β in order to confirm the accuracy of the solution procedure. According to the optimization results derived from the previous formulas, the basic optimal parameter values are provided in Table 1. The numerical solution of the harmonic excitation with excitation amplitude $F=1000N$ is obtained by using the fourth-order Runge–Kutta method when the calculation time is 2000 s. After the transient response is ignored, the greatest value of the steady-state solution is chosen as the excitation response amplitude and normalized. The normalized amplitude–frequency curves of the numerical and analytical solutions to the system are shown in Figure 6. The circle represents the numerical solution and the solid line represents the analytical solution. Various colors signify the selection of certain parameters. It can be seen intuitively from the

figures that two kinds of solutions are completely consistent under the same case, which proves the correctness of each parameter expression solved in this paper.

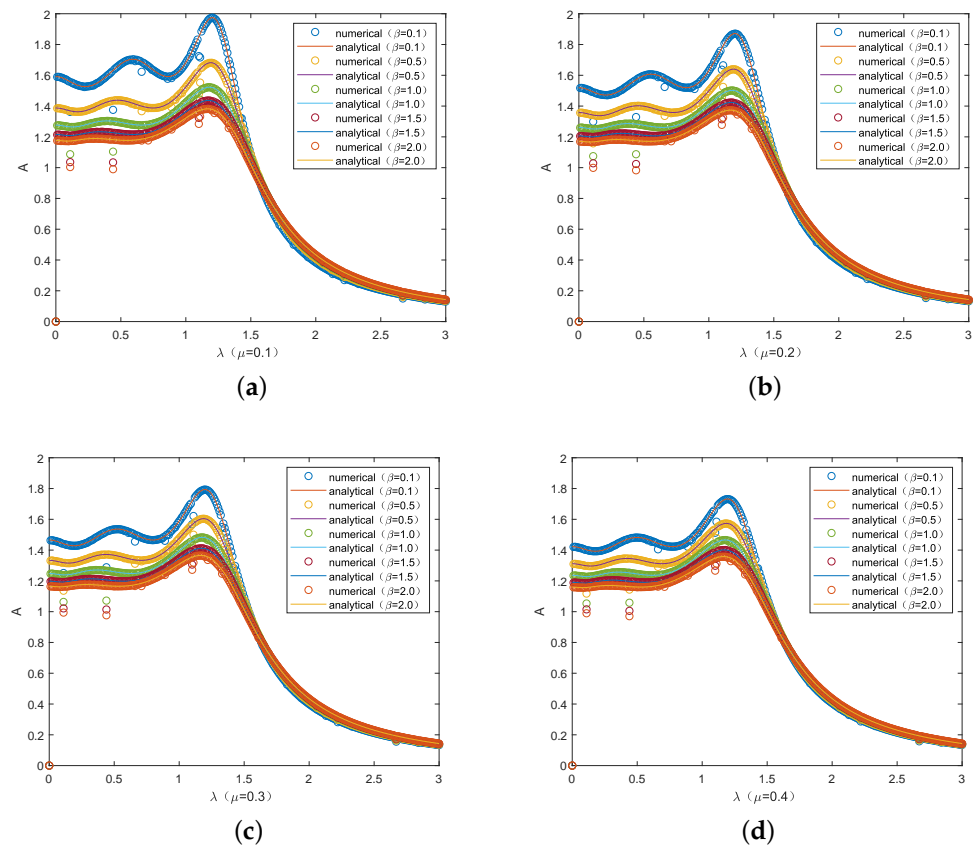


Figure 6. Comparison between the numerical solution and analytical solution in initial optimization ($\alpha_{2opt} = \alpha_{2b}$): (a) $\mu = 0.1$; (b) $\mu = 0.2$; (c) $\mu = 0.3$; (d) $\mu = 0.4$.

From the macroscopic perspective, the normalized amplitude amplification factor A of the primary system can be reduced by increasing the value of the inerter-to-mass ratio β under the same parameter μ . Meanwhile, the distance between the transverse coordinates corresponding to the peaks becomes larger. In a word, the larger the inerter-to-mass ratio is, the smaller the amplitude of the system is and the wider the frequency band is. By simply drawing the amplitude–frequency curves and obtaining the parameters, two different situations of parameter α_2 have different effects. It can be found that the distance between the vertical coordinates of the two formants in case $\alpha_{2opt} = \alpha_{2d}$ is closer than that in case $\alpha_{2opt} = \alpha_{2b}$. However, for the details, the fitting effect of the graph in $\alpha_{2opt} = \alpha_{2b}$ is better than $\alpha_{2opt} = \alpha_{2d}$. The main reason is that only when $\alpha_{2d} > -0.1150$, the ordinate of the initial position will gradually become lower than two resonance peaks, and the other results are not particularly ideal. Therefore, we consider the case of $\alpha_{2opt} = \alpha_{2b}$ in further optimization analysis. However, it is worth noting that there are some deviations in the solution process of this parameter. In the following part of the paper, we will introduce the PSO algorithm to further optimize the parameters, so as to make the two formants reach the horizontal height under certain parameter conditions.

Table 1. The specific parameters of the system with different inerter-to-mass ratios in initial optimization ($\alpha_{2opt} = \alpha_{2b}$).

Case 1: $\mu = 0.1, \alpha_{2opt} = \alpha_{2b}$	
$\beta = 0.1$	$\alpha_1 = 0.2094, \alpha_2 = -0.1078, \nu = 1.2320, \zeta = 0.6389$
$\beta = 0.5$	$\alpha_1 = 0.5405, \alpha_2 = -0.1061, \nu = 1.3079, \zeta = 1.3554$
$\beta = 1.0$	$\alpha_1 = 0.8209, \alpha_2 = -0.0909, \nu = 1.2516, \zeta = 1.9951$
$\beta = 1.5$	$\alpha_1 = 1.0125, \alpha_2 = -0.0780, \nu = 1.1794, \zeta = 2.5051$
$\beta = 2.0$	$\alpha_1 = 1.1511, \alpha_2 = -0.0679, \nu = 1.1124, \zeta = 2.9397$
Case 2: $\mu = 0.2, \alpha_{2opt} = \alpha_{2b}$	
$\beta = 0.1$	$\alpha_1 = 0.3037, \alpha_2 = -0.1110, \nu = 0.9063, \zeta = 0.6002$
$\beta = 0.5$	$\alpha_1 = 0.6063, \alpha_2 = -0.1031, \nu = 0.9200, \zeta = 1.0597$
$\beta = 1.0$	$\alpha_1 = 0.8648, \alpha_2 = -0.0880, \nu = 0.8749, \zeta = 1.4885$
$\beta = 1.5$	$\alpha_1 = 1.0437, \alpha_2 = -0.0757, \nu = 0.8241, \zeta = 1.8364$
$\beta = 2.0$	$\alpha_1 = 1.1744, \alpha_2 = -0.0661, \nu = 0.7778, \zeta = 2.1355$
Case 3: $\mu = 0.3, \alpha_{2opt} = \alpha_{2b}$	
$\beta = 0.1$	$\alpha_1 = 0.3899, \alpha_2 = -0.1106, \nu = 0.7523, \zeta = 0.5969$
$\beta = 0.5$	$\alpha_1 = 0.6667, \alpha_2 = -0.1000, \nu = 0.7454, \zeta = 0.9428$
$\beta = 1.0$	$\alpha_1 = 0.9057, \alpha_2 = -0.0853, \nu = 0.7059, \zeta = 1.2763$
$\beta = 1.5$	$\alpha_1 = 1.0730, \alpha_2 = -0.0736, \nu = 0.6649, \zeta = 1.5509$
$\beta = 2.0$	$\alpha_1 = 1.1964, \alpha_2 = -0.0645, \nu = 0.6281, \zeta = 1.7889$
Case 4: $\mu = 0.4, \alpha_{2opt} = \alpha_{2b}$	
$\beta = 0.1$	$\alpha_1 = 0.4686, \alpha_2 = -0.1087, \nu = 0.6548, \zeta = 0.6007$
$\beta = 0.5$	$\alpha_1 = 0.7222, \alpha_2 = -0.0969, \nu = 0.6395, \zeta = 0.8799$
$\beta = 1.0$	$\alpha_1 = 0.9437, \alpha_2 = -0.0827, \nu = 0.6040, \zeta = 1.1561$
$\beta = 1.5$	$\alpha_1 = 1.1006, \alpha_2 = -0.0716, \nu = 0.5691, \zeta = 1.3865$
$\beta = 2.0$	$\alpha_1 = 1.2172, \alpha_2 = -0.0629, \nu = 0.5380, \zeta = 1.5876$

3. Further Optimization Analysis of Particle Swarm Optimization Algorithm

This section studies the further parameter optimization problem of Maxwell-type DVA involving inerters and negative stiffness elements when the external excitation is harmonic excitation. In the previous part, we followed the H_∞ optimization criterion and obtained the approximate optimal solution of the model parameters using the fixed-point theory. Considering the practical engineering applications, the slight difference in parameter values may cause different effects. The numerical simulation using the Runge–Kutta method shows that the approximate optimal solution does not make the resonance peak at the same level, which indicates that the parameters of the model are worth further optimizing. It should be emphasized that the approximate optimal solution obtained by theoretical analysis plays a crucial part in introducing the PSO algorithm in this section, because only when a range is roughly determined can the process of algorithm iteration be infinitely close to the optimal value.

3.1. Optimizing the Single Variable

There are many parameters that can be adjusted in the model. We first check to see if adjusting the single variable can minimize the maximum amplitude of the primary system. Here, the amplitude of the primary system is selected as the objective function, and the PSO algorithm is employed to optimize it. The condition of the algorithm is that the dimension of the selected particle is 1; that is, the parameter ζ to be determined. The values of parameters other than ζ are the same as those in Table 1 according to the settings of μ and β . In order to obtain more accurate vibration absorption parameters, we set the following: (1) there are 40 particles in total; (2) the maximum number of iterations is 1000; (3) the learning factors c_1 and c_2 are both 2; (4) the maximum and minimum values of inertia weight are 0.6 and 0.4; (5) the random number sequence in the population is added; (6) the position and velocity of particles have a definite proportional connection.

The initial state of the algorithm is a group of random particles with two attributes, velocity and position. The particles update their velocity vector and position vector by continuously tracking the individual optimal value and global optimal value. Specifically, the particle will store the magnitude and direction of the preceding velocity in memory and self-recognize the current point with its own best point while completing group cognition with the best point in the population. In this way, each particle achieves collaboration and optimal solution information sharing between populations. When the maximum number of iterations is set, the particle swarm can seek the best position according to the termination condition of iterations and output the ideal parameter values. By analyzing the rule of the amplitude curves, the system will produce two wave peaks depending on the parameter values, and the two peaks will reach equal height when the parameters are optimal. When designing the PSO algorithm, the maximum values of the amplitude curve of the i -th iteration are obtained first, and then the damping ratio that minimizes the maximum amplitude in all iterations is the optimal damping ratio under the single variable optimization we are looking for.

As shown in Table 2, we obtained more comprehensive values than in Table 1 according to the PSO algorithm after optimizing the single parameter ζ , including the maximum amplitude under the optimal parameter values, the abscissas λ (λ_{peak1} , λ_{peak2}) corresponding to the two peaks and the difference between them. From this information, we can see the following: (1) Under the same mass ratio μ , the value of the optimal damping ratio is larger than the approximate damping ratio obtained in the previous section with the increase in the inerter-to-mass ratio β , and the amplitude becomes smaller. The λ_{peak1} corresponding to the left peak gradually moves to the left. The λ_{peak2} corresponding to the right peak gradually moves to the right. The larger difference means that the resonance frequency band is getting wider, and the resonance effect is becoming better and more stable. (2) Under the same coefficient β , the system amplitude decreases slowly with the increase in μ and the abscissas λ (λ_{peak1} , λ_{peak2}) become wider. This is consistent with the results of other scholars, who found that mass ratio can effectively suppress the amplitude of the system when studying vibration absorbers.

It can be clearly observed in Figures 6 and 7 that the amplitude of the system after optimization is significantly reduced, showing better stability. Moreover, the number of iterations largely determines the accuracy of the optimal value. The amplitude of the primary system finally tends to a straight line after 1000 iterations using PSO from Figure 8. At the initial iteration, a specific downward trend in the amplitude change can be seen from the enlarged color section. It should be noted here that the minimum number of iterations at which the amplitude flattens out is not the optimal number of iterations. Different iterations make the amplitude have different forms of decline. According to the final stationary state in the figure, the mass ratio can suppress the amplitude under the same inerter parameters. The range of parameter given during the iteration is critical, which determines whether the identified optimal value is reliable. We also calculate the mean square response of the primary system before and after optimizing the single parameter ζ . Taking $\mu = 0.1$ as an example, the optimized mean square response outperforms the value before optimization with the same parameter β . With the increase in β , the response before and after optimization is gradually reduced. The mean square response reflects the dispersion degree of individuals in the data set and can be used as a result to measure the degree of system distribution. For example, two data with the same mean may not have the same mean square response. If the overall mean square response value is low, it can be judged that its stability is also good.

Table 2. The specific parameters of the system in different cases of the inerter-to-mass ratio when optimizing the single variable ζ ($\alpha_{2opt} = \alpha_{2b}$).

Case 1: $\mu = 0.1$								
β	ζ_{ori}	$\sigma_{ori}^2(\frac{\pi S_0}{\omega_1^3})$	ζ_{opt}	$\sigma_{opt}^2(\frac{\pi S_0}{\omega_1^3})$	A_{max}	λ_{peak1}	λ_{peak2}	$ \lambda_{peak1} - \lambda_{peak2} $
0.1	0.6389	2.7821	0.7063	2.7370	1.8288	0.625	1.234	0.609
0.5	1.3554	2.2072	1.5275	2.1358	1.5391	0.517	1.243	0.726
1.0	1.9951	1.9117	2.2771	1.8269	1.3865	0.437	1.249	0.812
1.5	2.5051	1.7570	2.8845	1.6649	1.3046	0.383	1.253	0.870
2.0	2.9397	1.6612	3.4085	1.5641	1.2529	0.344	1.257	0.913
Case 2: $\mu = 0.2$								
β	ζ_{ori}	$\sigma_{ori}^2(\frac{\pi S_0}{\omega_1^3})$	ζ_{opt}	$\sigma_{opt}^2(\frac{\pi S_0}{\omega_1^3})$	A_{max}	λ_{peak1}	λ_{peak2}	$ \lambda_{peak1} - \lambda_{peak2} $
0.1	0.6002	2.5747	0.6679	2.5200	1.7248	0.591	1.237	0.646
0.5	1.0597	2.1280	1.1979	2.0531	1.4986	0.498	1.244	0.746
1.0	1.4885	1.8735	1.7022	1.7870	1.3664	0.425	1.250	0.825
1.5	1.8364	1.7344	2.1177	1.6411	1.2925	0.375	1.254	0.879
2.0	2.1355	1.6463	2.4791	1.5483	1.2447	0.337	1.258	0.921
Case 3: $\mu = 0.3$								
β	ζ_{ori}	$\sigma_{ori}^2(\frac{\pi S_0}{\omega_1^3})$	ζ_{opt}	$\sigma_{opt}^2(\frac{\pi S_0}{\omega_1^3})$	A_{max}	λ_{peak1}	λ_{peak2}	$ \lambda_{peak1} - \lambda_{peak2} $
0.1	0.5969	2.4220	0.6677	2.3602	1.6480	0.563	1.239	0.676
0.5	0.9428	2.0613	1.0687	1.9834	1.4642	0.481	1.245	0.764
1.0	1.2763	1.8396	1.4623	1.7515	1.3485	0.413	1.251	0.838
1.5	1.5509	1.7138	1.7910	1.6195	1.2814	0.366	1.255	0.889
2.0	1.7889	1.6324	2.0792	1.5336	1.2371	0.331	1.259	0.928
Case 4: $\mu = 0.4$								
β	ζ_{ori}	$\sigma_{ori}^2(\frac{\pi S_0}{\omega_1^3})$	ζ_{opt}	$\sigma_{opt}^2(\frac{\pi S_0}{\omega_1^3})$	A_{max}	λ_{peak1}	λ_{peak2}	$ \lambda_{peak1} - \lambda_{peak2} $
0.1	0.6007	2.3031	0.6746	2.2359	1.5878	0.539	1.241	0.702
0.5	0.8799	2.0043	0.9999	1.9237	1.4347	0.465	1.247	0.782
1.0	1.1561	1.8092	1.3269	1.7196	1.3324	0.403	1.252	0.849
1.5	1.3865	1.6948	1.6034	1.5995	1.2711	0.359	1.256	0.897
2.0	1.5876	1.6194	1.8474	1.5199	1.2300	0.325	1.260	0.935

In addition to optimizing the single variable ζ , the parameters ν , α_1 , and α_2 can also be considered as the case of optimizing the single variable. The following Table 3 shows the system’s optimal target, the abscissa λ ($\lambda_{peak}, \lambda_{peak1}, \lambda_{peak2}$) corresponding to the amplitude and the mean square response after optimizing the single variables ν , α_1 , and α_2 respectively. From the perspective of system amplitude, the maximum amplitudes optimized by these three single variables are all higher than the optimization results of ζ under the same μ and β . The optimization of ζ can better minimize the maximum amplitude of the primary system under the single-parameter optimization. However, the mean square response of optimized ν is the best, and the difference between the abscissas corresponding to the two peaks is larger (as manifested in Appendix Table A1). It can be seen from Figure 9 that the amplitude curves of the analytical solution and numerical solution decrease at the initial position under the optimization of ν , which is why the mean square response is lower. Through the detailed analysis of the four single parameters in this chapter, the conclusions we draw can be multifaceted. For the purpose of suppressing the amplitude of the primary system, the optimization parameter ζ is a better choice. If we want to make the mean square response value of the system lower, we can choose the optimization parameter ν . Therefore, it is concluded that the influence of different parameters on the system must exist. The algorithm is further optimized based on the fixed-point theory to make the discussion of the vibration absorber more accurate.

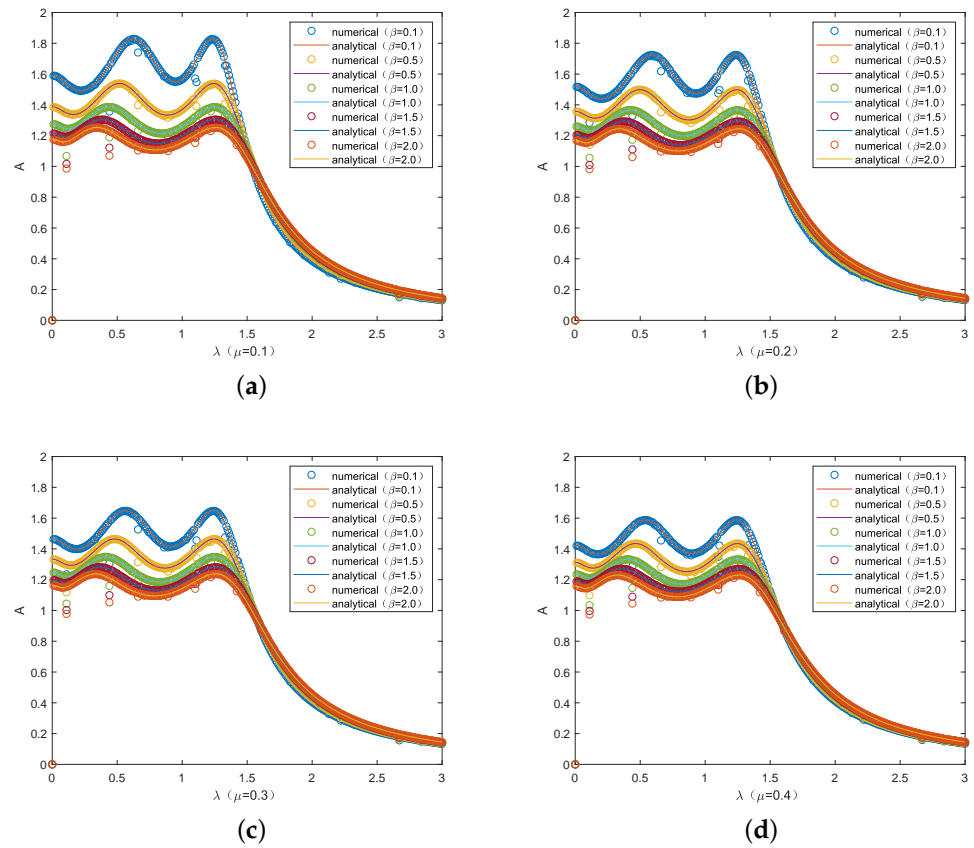


Figure 7. Comparison between the numerical solution and analytical solution when optimizing the single variable ζ ($\alpha_{2opt} = \alpha_{2b}$): (a) $\mu = 0.1$; (b) $\mu = 0.2$; (c) $\mu = 0.3$; (d) $\mu = 0.4$.

Table 3. The specific parameters of the system in different inerter-to-mass ratios when optimizing the other variables ($\alpha_{2opt} = \alpha_{2b}$, $\mu = 0.1$).

β	0.1	0.5	1.0	1.5	2.0
α_{1opt}	0.2428	0.6467	1.0072	1.2658	1.4591
A_{max}	1.9098	1.6181	1.4601	1.3744	1.3202
$\sigma_{opt}^2(\pi S_0/\omega_1^3)$	2.7754	2.1711	1.8560	1.6893	1.5853
λ_{peak}	1.142	1.099	1.061	1.034	1.013
β	0.1	0.5	1.0	1.5	2.0
α_{2opt}	−0.0981	−0.0733	−0.0302	0.0084	0.0424
A_{max}	1.8970	1.6372	1.4954	1.4175	1.3677
$\sigma_{opt}^2(\pi S_0/\omega_1^3)$	2.8039	2.2305	1.9323	1.7746	1.6764
λ_{peak1}	0.617	0.517	0.447	0.402	0.370
λ_{peak2}	1.209	1.195	1.182	1.174	1.168
$ \lambda_{peak1} - \lambda_{peak2} $	0.592	0.678	0.735	0.772	0.798
β	0.1	0.5	1.0	1.5	2.0
ν_{opt}	1.2617	1.3753	1.3464	1.2903	1.2333
A_{max}	1.8373	1.5504	1.3971	1.3138	1.2607
$\sigma_{opt}^2(\pi S_0/\omega_1^3)$	2.7349	2.1274	1.8151	1.6516	1.5503
λ_{peak1}	0.588	0.459	0.368	0.309	0.268
λ_{peak2}	1.230	1.240	1.247	1.253	1.258
$ \lambda_{peak1} - \lambda_{peak2} $	0.642	0.781	0.879	0.944	0.990

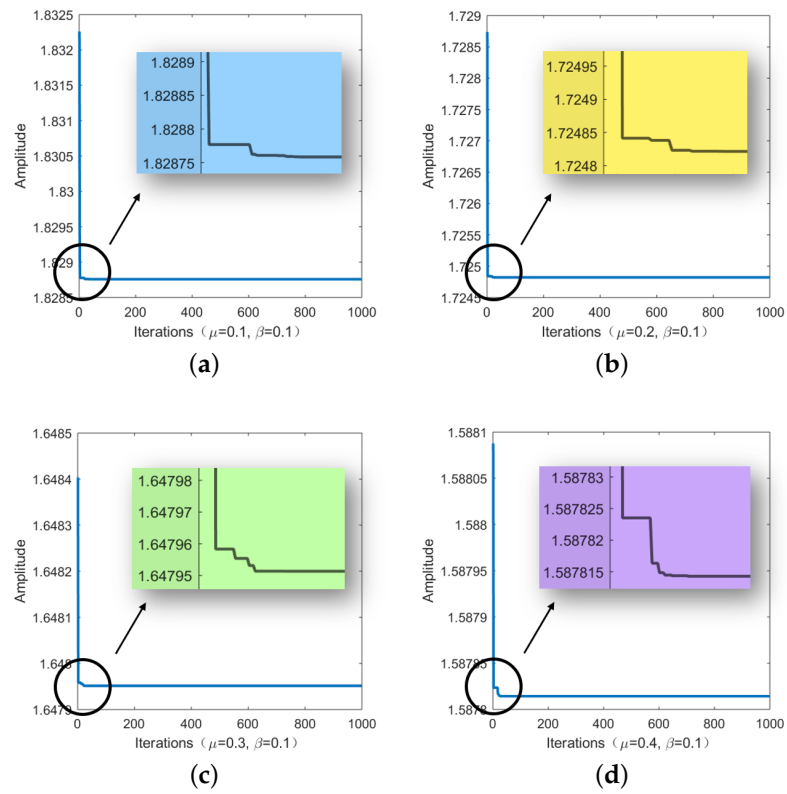


Figure 8. Iterations when optimizing the single variable ζ ($\alpha_{2opt} = \alpha_{2b}$, $\beta = 0.1$): (a) $\mu = 0.1$; (b) $\mu = 0.2$; (c) $\mu = 0.3$; (d) $\mu = 0.4$.

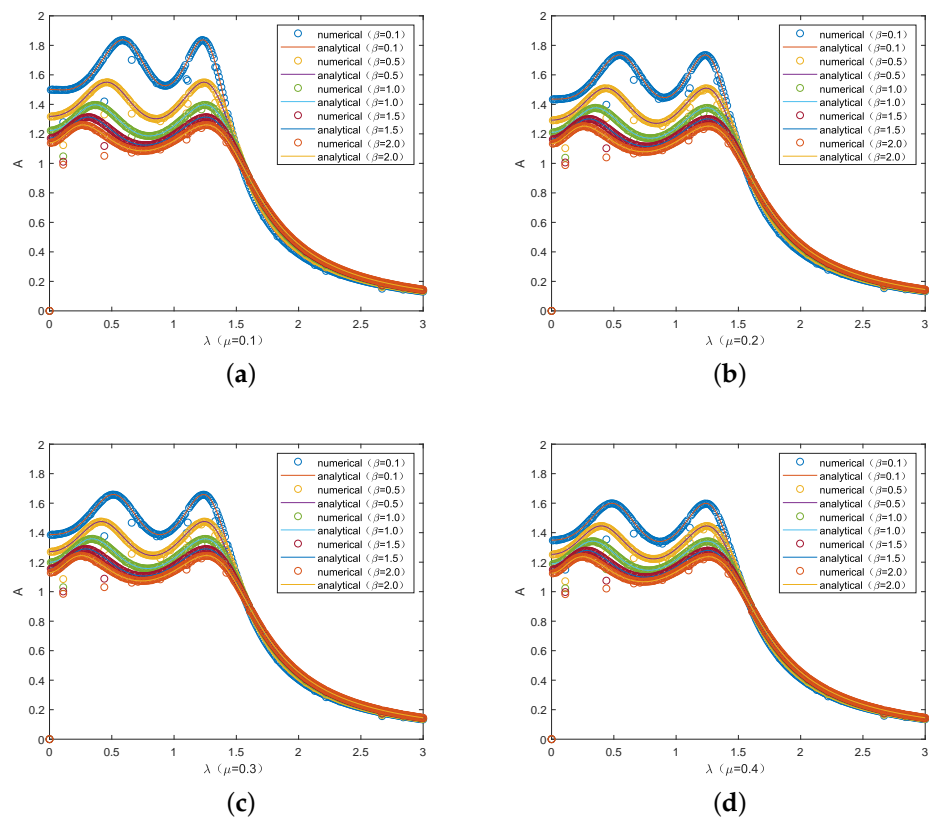


Figure 9. Comparison between the numerical solution and analytical solution when optimizing the single variable ν ($\alpha_{2opt} = \alpha_{2b}$): (a) $\mu = 0.1$; (b) $\mu = 0.2$; (c) $\mu = 0.3$; (d) $\mu = 0.4$.

3.2. Optimizing Four Variables: α_1, α_2, ν , and ζ

This section will simultaneously optimize four variables to observe the variation in the system amplitude curve and the degree of mean square response. The difficulty lies in the need to consider the value range of four parameter values at the same time. The optimized parameter value cannot be located at the endpoint value of the range, nor can the parameter value only meet part of the value range. The setting of the value range about the four parameter values is based on the range considered in the previous optimization of the single variable, which ensures that the optimal value obtained after the comprehensive optimization is comparable to the optimal value of the optimized single variable and further judges the iterative optimization efficiency of the PSO algorithm. The values of α_1 and α_2 (as shown in Table 4) are higher than those before optimization in Table 1. The values of ν and ζ are between the approximate optimal value before optimization and the optimal value after single optimization.

Table 4. The specific parameters of the system in different cases of inerter-to-mass ratio when optimizing four variables, α_1, α_2, ν , and ζ ($\alpha_{2opt} = \alpha_{2b}$).

Case 1: $\mu = 0.1$								
β	α_{1opt}	α_{2opt}	ν_{opt}	ζ_{opt}	A_{max}	$A_{max(all-\zeta)}$	$A_{max(all-\nu)}$	$\sigma_{opt}^2(\frac{\pi S_0}{\omega_1^3})$
0.1	0.2346	-0.1045	1.2346	0.6612	1.8151	-0.0137	-0.0222	2.7579
0.5	0.5898	-0.1010	1.3242	1.4165	1.5269	-0.0122	-0.0235	2.1360
1.0	0.9062	-0.0792	1.2712	2.0833	1.3821	-0.0044	-0.0150	1.8276
1.5	1.1576	-0.0664	1.2005	2.6207	1.2930	-0.0116	-0.0208	1.6546
2.0	1.3392	-0.0576	1.1368	3.0753	1.2375	-0.0154	-0.0232	1.5467
Case 2: $\mu = 0.2$								
β	α_{1opt}	α_{2opt}	ν_{opt}	ζ_{opt}	A_{max}	$A_{max(all-\zeta)}$	$A_{max(all-\nu)}$	$\sigma_{opt}^2(\frac{\pi S_0}{\omega_1^3})$
0.1	0.3249	-0.1047	0.9086	0.6224	1.7311	0.0063	-0.0037	2.5447
0.5	0.6497	-0.0968	0.9300	1.1182	1.4921	-0.0065	-0.0178	2.0559
1.0	0.9437	-0.0825	0.8868	1.5852	1.3520	-0.0144	-0.0248	1.7799
1.5	1.1789	-0.0666	0.8424	1.9237	1.2782	-0.0143	-0.0232	1.6288
2.0	1.3677	-0.0560	0.7942	2.2385	1.2290	-0.0157	-0.0233	1.5306
Case 3: $\mu = 0.3$								
β	α_{1opt}	α_{2opt}	ν_{opt}	ζ_{opt}	A_{max}	$A_{max(all-\zeta)}$	$A_{max(all-\nu)}$	$\sigma_{opt}^2(\frac{\pi S_0}{\omega_1^3})$
0.1	0.4079	-0.1030	0.7544	0.6267	1.6603	0.0123	0.0016	2.3830
0.5	0.7113	-0.0950	0.7547	1.0015	1.4545	-0.0097	-0.0210	1.9817
1.0	1.0262	-0.0754	0.7199	1.3287	1.3365	-0.0120	-0.0221	1.7424
1.5	1.2059	-0.0648	0.6802	1.6278	1.2671	-0.0143	-0.0229	1.6073
2.0	1.4099	-0.0507	0.6371	1.8823	1.2249	-0.0122	-0.0196	1.5177
Case 4: $\mu = 0.4$								
β	α_{1opt}	α_{2opt}	ν_{opt}	ζ_{opt}	A_{max}	$A_{max(all-\zeta)}$	$A_{max(all-\nu)}$	$\sigma_{opt}^2(\frac{\pi S_0}{\omega_1^3})$
0.1	0.4877	-0.1009	0.6595	0.6312	1.5985	0.0107	-0.0005	2.2532
0.5	0.7599	-0.0912	0.6441	0.9496	1.4289	-0.0058	-0.0169	1.9254
1.0	1.0724	-0.0694	0.6149	1.2030	1.3251	-0.0073	-0.0171	1.7141
1.5	1.2400	-0.0613	0.5801	1.4608	1.2584	-0.0127	-0.0211	1.5889
2.0	1.4140	-0.0528	0.5505	1.6637	1.2143	-0.0157	-0.0228	1.5020

From the perspective of amplitude, the amplitude amplification factor obtained by optimizing four variables at the same time is better than that obtained by optimizing single variables ν and ζ except for a few cases. From the perspective of the mean square response, it is better than optimizing the single variable ζ but inferior to the single variable ν . This conclusion holds in most cases and cannot be applied to all cases of μ and β . As can be seen from Figure 10 of the analytical and numerical solutions, the amplitude–frequency curves of the four variables optimized at the same time have a lower amplitude than ζ at the starting position, just like the single variable ν . At the trough between the two peaks, its steepness is less than that of the optimized single variable ν or ζ , and the stationarity

looks smoother. In sum, whether optimizing a single variable or four variables, there are advantages and disadvantages. If four variables are selected to be optimized at the same time, the value range of each variable needs to be determined by optimizing the single variable, which increases the time cost of numerical simulation. In practical engineering applications, we need to combine the actual conditions and technical methods to select the appropriate optimization method. It is advisable to select a single variable or optimize several variables.

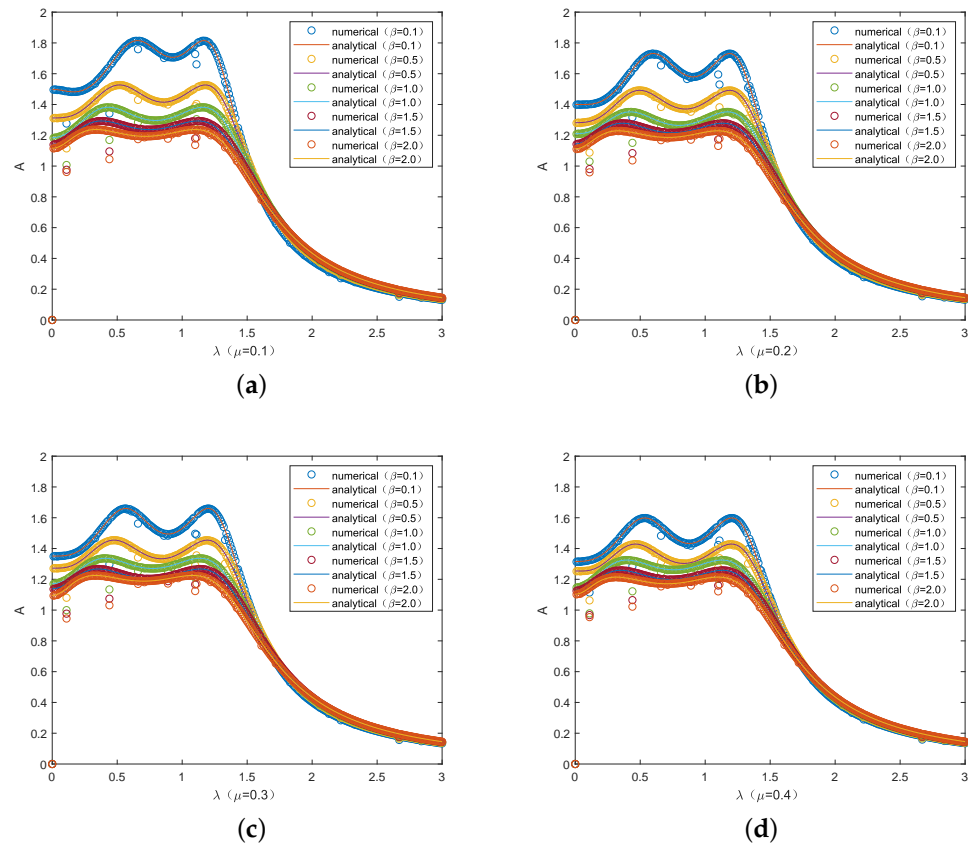


Figure 10. Comparison between numerical solution and analytical solution when optimizing four variables, α_1 , α_2 , ν , and ζ , at the same time: (a) $\mu = 0.1$; (b) $\mu = 0.2$; (c) $\mu = 0.3$; (d) $\mu = 0.4$.

3.3. Validity of Parameter Selection

Figure 11 shows the effectiveness of parameters after optimizing variable ζ according to the changes in different parameters in the system. When the value of μ and β are respectively increased, the corresponding amplitude curves not only show low resonance response peaks but also have a large impact on the vibration reduction bandwidth (as displayed in Figure 11a,b). On the premise of taking the optimal value as a reference, the numerical simulation is carried out by selecting its adjacent values to obtain the Figure 11c–f). The most obvious thing is that the orange line represents the curve at the optimal value and is consistent with the results obtained. Other curves have the following properties: (1) the left peak and the right peak are not at the same level; (2) the influence of the parameter value on the vibration reduction bandwidth exists; (3) different parameters affect the position of the initial point of the curve, which may be smaller or infinite; (4) the system will be over-damped, thus affecting the robustness under excitation.

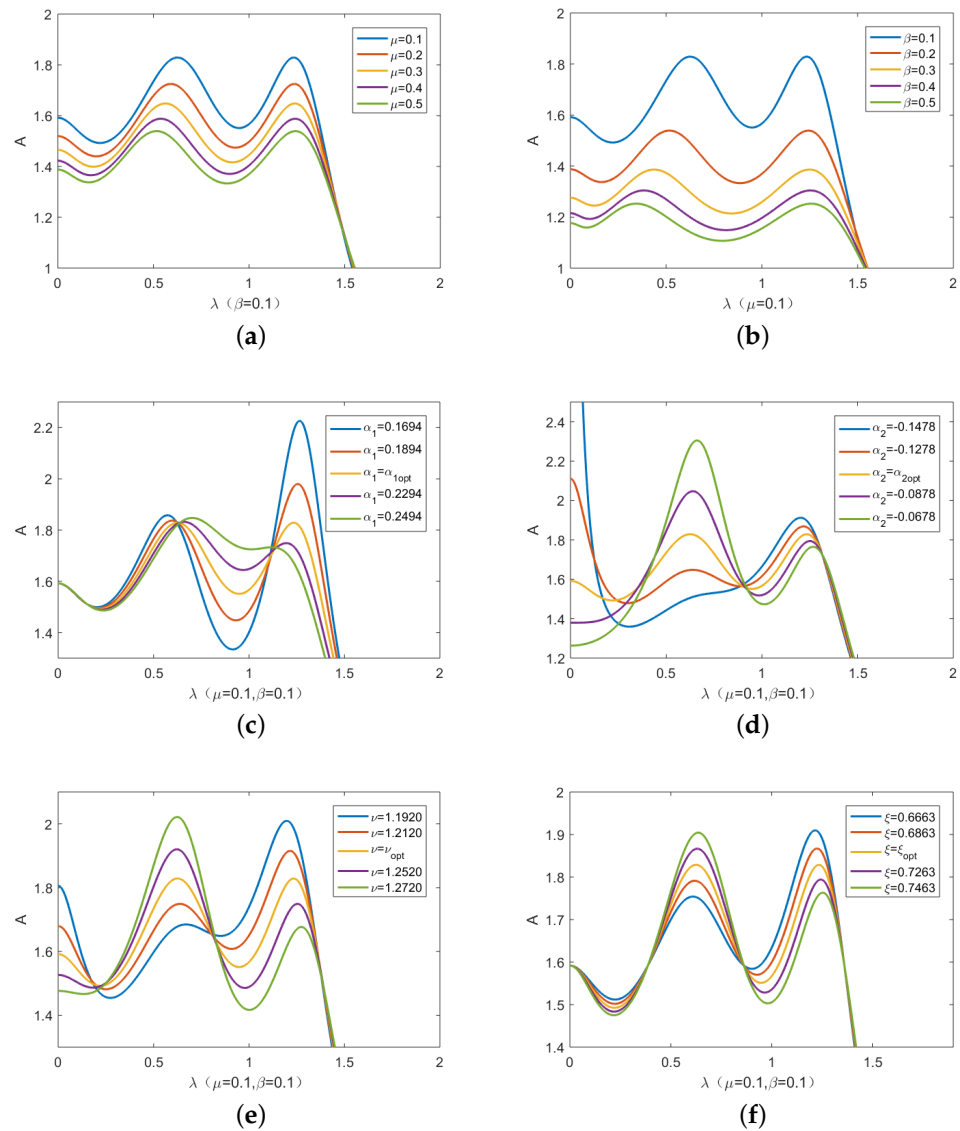


Figure 11. The optimal parameters verification when optimizing the single variable ζ : (a) change μ ; (b) change β ; (c) change α_1 ; (d) change α_2 ; (e) change ν ; (f) change ζ .

4. The Mean Square Responses of the Primary System for Different DVAs

In nature and engineering, there is a class of vibration sources that cannot be described in a certain time and space, such as earthquakes, turbulence, noise, etc., which are called random vibration sources. Usually, the random vibration in structural dynamics is analyzed for stationary random processes. The difference between it and non-stationary random processes is whether the statistics such as mean and variance change with time. Due to the limitation of some necessary conditions, it is almost impossible for us to study the influence of the whole random process on the system, so we adopt the form of partial random vibration samples in the analysis process. This section explores the DVA under random excitation in more detail and uses comparisons to show how effective the design is. We determine the power spectral density functions $S(\omega)$ attached to various DVAs by considering the primary system under random excitation. The subscripts D, R, A, W, AN, WN, and M stand for the Voigt-type DVA, Ren model, Asami model, Wang model, Asami model with negative stiffness, Wang model with negative stiffness, and the DVA in this study. These models can be found in Figure 12. Based on the equations of each model, the

mean square responses of the primary system under different DVAs can be calculated as follows.

$$\begin{aligned} \sigma_D^2 &= \int_{-\infty}^{+\infty} S_D(\omega) d\omega = S_0 \int_{-\infty}^{+\infty} \|H_{Dx_1}(j\omega)\|^2 d\omega = \frac{\pi S_0 Y_D}{2\omega_1^3 \mu \zeta v} \\ \sigma_R^2 &= \int_{-\infty}^{+\infty} S_R(\omega) d\omega = S_0 \int_{-\infty}^{+\infty} \|H_{Rx_1}(j\omega)\|^2 d\omega = \frac{\pi S_0 Y_R}{2\omega_1^3 \mu \zeta v^5} \\ \sigma_A^2 &= \int_{-\infty}^{+\infty} S_A(\omega) d\omega = S_0 \int_{-\infty}^{+\infty} \|H_{Ax_1}(j\omega)\|^2 d\omega = \frac{\pi S_0 Y_A}{2\omega_1^3 \mu \zeta \alpha^2 v^3} \\ \sigma_W^2 &= \int_{-\infty}^{+\infty} S_W(\omega) d\omega = S_0 \int_{-\infty}^{+\infty} \|H_{Wx_1}(j\omega)\|^2 d\omega = \frac{\pi S_0 Y_W}{2\omega_1^3 \mu \zeta \alpha^2 v^7} \\ \sigma_{AN}^2 &= \int_{-\infty}^{+\infty} S_{AN}(\omega) d\omega = S_0 \int_{-\infty}^{+\infty} \|H_{ANx_1}(j\omega)\|^2 d\omega \\ &= \frac{\pi S_0 Y_{AN}}{2\omega_1^3 \mu \zeta \alpha_1^2 v^3 (1 - \alpha_2 v^2)^2 (1 + \alpha_2 + \mu \alpha_2 v^2)} \\ \sigma_{WN}^2 &= \int_{-\infty}^{+\infty} S_{WN}(\omega) d\omega = S_0 \int_{-\infty}^{+\infty} \|H_{WNx_1}(j\omega)\|^2 d\omega \\ &= \frac{\pi S_0 Y_{WN}}{2\omega_1^3 \mu \zeta \alpha_1^2 v^7 (1 + \alpha_2 + \mu \alpha_2 v^2)} \\ \sigma_M^2 &= \int_{-\infty}^{+\infty} S_M(\omega) d\omega = S_0 \int_{-\infty}^{+\infty} \|H_{Mx_1}(j\omega)\|^2 d\omega \\ &= \frac{\pi S_0 Y_M}{2\omega_1^3 \mu \zeta \alpha_1^2 v (\mu + \beta - \alpha_2)^2 [\alpha_2 + (1 + \alpha_2) \mu v^2]} \end{aligned}$$

where

$$\begin{aligned} Y_D &= 1 + [4\zeta^2(1 + \mu) - \mu - 2]v^2 + (1 + \mu)^2 v^4 \\ Y_R &= 1 + (4\zeta^2 + \mu - 2)v^2 + v^4 \\ Y_A &= 4\zeta^2 \{1 + (1 + \alpha) [-2 + (1 + \alpha)(1 + \mu)v^2] v^2\} \\ &\quad + \alpha^2 v^2 [1 - (2 + \mu)v^2 + (1 + \mu)^2 v^4] \\ Y_W &= 4\zeta^2 \{1 - 2(1 + \alpha - \mu)v^2 + [(1 + \alpha)^2 - (1 + 2\alpha)\mu + \mu^2] v^4\} \\ &\quad + \alpha^2 v^2 [1 + (\mu - 2)v^2 + v^4] \\ Y_{AN} &= 4\zeta^2 (1 + \alpha_2 + \alpha_2 \mu v^2) \{1 - 2(1 + \alpha_1 + \alpha_2)v^2 + [(1 + \alpha_1 + \alpha_2)^2 + \mu(1 + \alpha_1)^2] v^4\} \\ &\quad + \alpha_1^2 v^2 \{1 + \alpha_2 - [2(1 + \alpha_2)^2 + \mu] v^2 + [(1 + \alpha_2)^3 + 2(1 + \alpha_2)\mu + \mu^2] v^4\} \\ Y_{WN} &= 4\zeta^2 (1 + \alpha_2 + \alpha_2 \mu v^2) \{1 - 2(1 + \alpha_1 + \alpha_2 - \mu)v^2 + [(1 + \alpha_1 + \alpha_2)^2 \\ &\quad - (1 + 2\alpha_1 + 2\alpha_2)\mu + \mu^2] v^4\} + \alpha_1^2 v^2 \{1 + \alpha_2 + [-2(1 + \alpha_2)^2 \\ &\quad + \mu(1 + 2\alpha_2)] v^2 + [(1 + \alpha_2)^3 - 2\alpha_2(1 + \alpha_2)\mu + \alpha_2 \mu^2] v^4\} \\ Y_M &= \alpha_1^2 (\mu v^2 + \alpha_2)^2 [\alpha_2 + (\mu + \beta)^2 + \mu v^2 (1 + \mu + \beta)^2] \\ &\quad + [\alpha_2 + (1 + \alpha_2) \mu v^2] \{4\zeta^2 \mu^2 v^2 (\mu + \beta) (\mu + \beta + \alpha_2^2) \\ &\quad + (1 + \alpha_2) (\mu + \beta) [\alpha_1^2 (\mu + \beta) - 8\zeta^2 \mu^2 v^2 (\mu v^2 + \alpha_1 + \alpha_2)] \\ &\quad - 2(1 + \mu + \beta) [\alpha_1^2 (\mu + \beta) (\mu v^2 + \alpha_2) - 2\zeta^2 \mu^2 v^2 (\mu v^2 + \alpha_1 + \alpha_2)^2]\} \end{aligned}$$

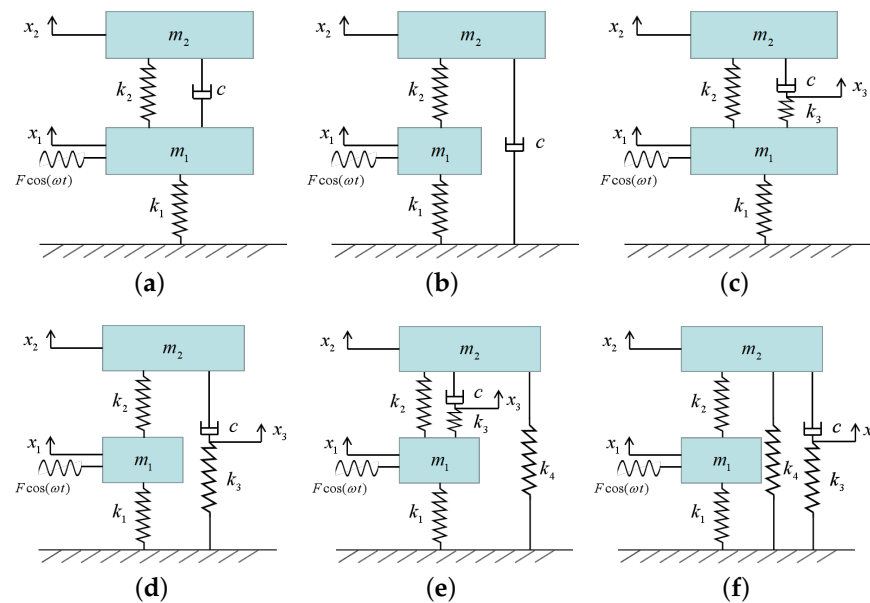


Figure 12. The DVA models: (a) Den; (b) Ren; (c) Asami; (d) Wang; (e) Asami with negative stiffness; (f) Wang with negative stiffness.

According to the optimal parameters in the literature [1,5,6,17,33,34], the mean square responses of the primary systems when $\mu = 0.1$ can be obtained as

$$\sigma_D^2 = \frac{6.401\pi S_0}{\omega_1^3}, \sigma_R^2 = \frac{5.780\pi S_0}{\omega_1^3}, \sigma_A^2 = \frac{6.039\pi S_0}{\omega_1^3}$$

$$\sigma_W^2 = \frac{7.065\pi S_0}{\omega_1^3}, \sigma_{AN}^2 = \frac{3.095\pi S_0}{\omega_1^3}, \sigma_{WN}^2 = \frac{3.090\pi S_0}{\omega_1^3}$$

In the previous section, we calculated the mean square responses by optimizing the single variable and four variables. It was found that the three cases studied in this paper are better than the above comparison models. This demonstrates that the model achieves better results than other DVAs under random excitation, and the inerter is crucial to the model. In addition, the model still outperforms the other DVAs when different mass ratios are selected. When random excitation is selected, 5000 normalized random numbers with zero mean value and unit variance are created as a 50 s random excitation (as shown in Figure 13). Firstly, we investigate three cases based on particle swarm optimization (ζ, ν, all) in this paper to select one for comparison with other models. As in Figure 14, three cases have roughly the same trend in the curve direction, and each section does not have the rule of periodic vibration. By locating the coordinates of the three curve peaks, the maximum peak appears the most times when the single variable ζ is optimized, and optimizing the single variable ν appears the fewest times. In the preliminary conclusion obtained in the previous section, the amplitude amplification factor obtained by optimizing the four variables simultaneously is better than that obtained by optimizing the single variables ν and ζ in most cases. From the perspective of mean square response, it is superior to the optimization of single variable ζ but inferior to the single variable ν . Therefore, the optimization of the single variable ζ is weaker than the other two cases according to the judgment. If it is selected to compare with the other models, it indicates that the three cases of optimization about this model are applicable.

It can be clearly observed from Figure 15a that the influence of the vibration absorber on the primary system is very great. The displacement can be considerably decreased with its help. In the meantime, raising the inerter coefficient can lessen the primary system’s response for the model as shown in Figure 15b. According to the calculation of the model parameters in the existing literature, the fourth-order Runge–Kutta method is used to

determine the amplitude responses under different DVAs conditions. These time history diagrams can be seen in Figure 16. Because the displacement variance of the primary system is frequently related to the vibration energy, the variances and decreasing ratios of the displacements for different systems are compiled in Table 5. Under random excitation, the DVA discussed in this work performs with better control performance than other DVAs. These results demonstrate that the proposed DVA can lower the mean square response of the system as well as the response peak.

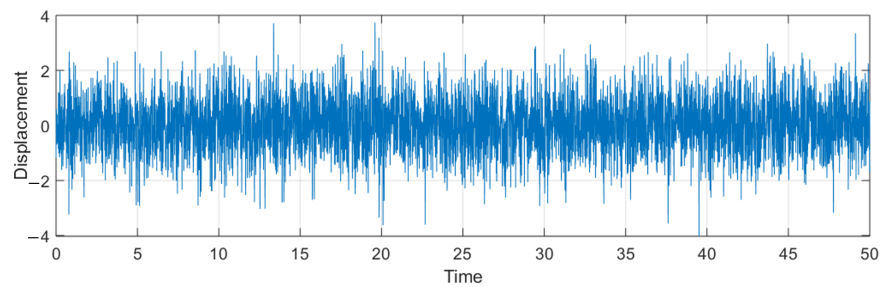


Figure 13. The time history of the random excitation.

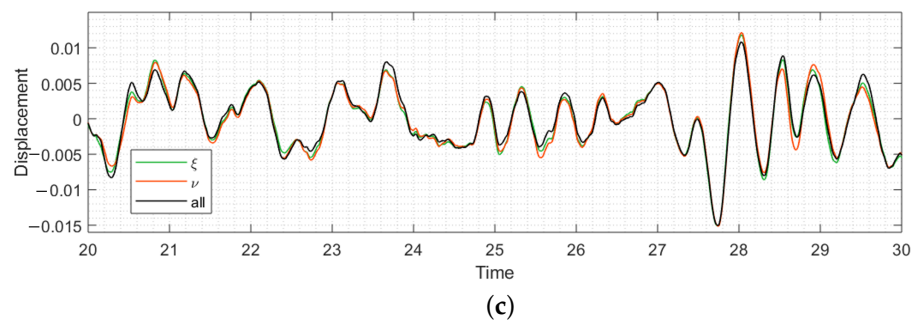
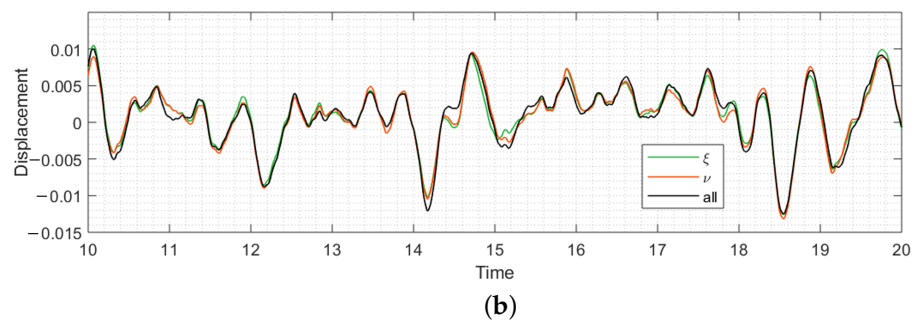
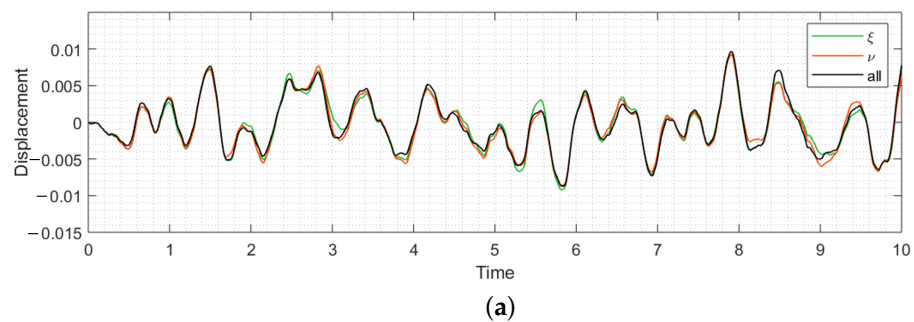
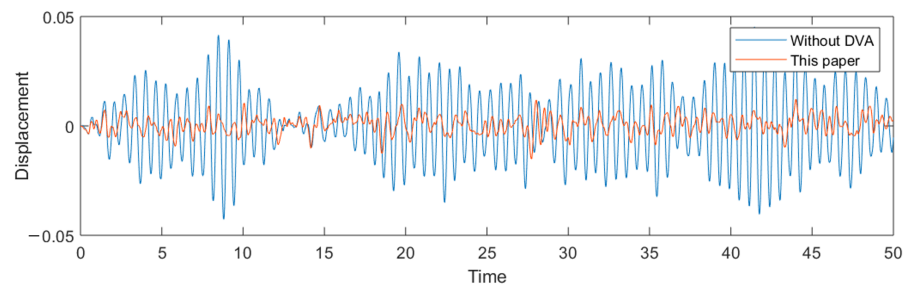


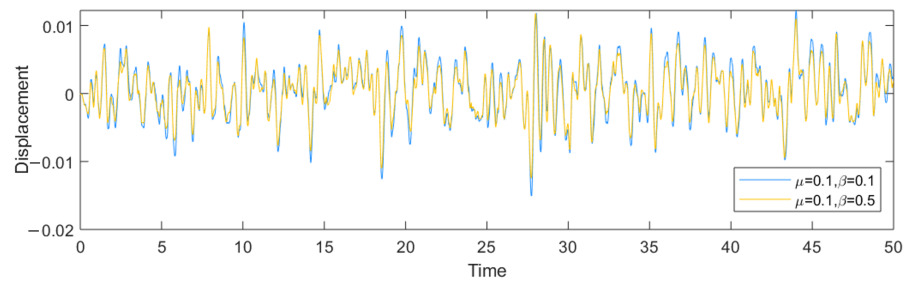
Figure 14. The time history of three cases based on particle swarm optimization (ξ , ν , all): (a) $t \in [0, 10]$; (b) $t \in [10, 20]$; (c) $t \in [20, 30]$.

Table 5. The variances and decreasing ratios of the displacements in the primary system.

Models	Variances	Decrease Ratios (%)
Without DVA	2.57202×10^{-4}	/
DVA by Den Hartog	3.73465×10^{-5}	85.48
DVA by Ren	3.36063×10^{-5}	86.93
DVA by Asami	3.37462×10^{-5}	86.88
DVA by Wang	4.12604×10^{-5}	83.96
DVA by Asami with negative stiffness	1.83878×10^{-5}	92.85
DVA by Wang with negative stiffness	1.86308×10^{-5}	92.76
The presented model ($\mu = 0.1, \beta = 0.1$)	1.60176×10^{-5}	93.77
The presented model ($\mu = 0.1, \beta = 0.5$)	1.26826×10^{-5}	95.07
The presented model ($\mu = 0.1, \beta = 1.0$)	1.10374×10^{-5}	95.71
The presented model ($\mu = 0.1, \beta = 1.5$)	9.66774×10^{-6}	96.24
The presented model ($\mu = 0.1, \beta = 2.0$)	9.16522×10^{-6}	96.44



(a)



(b)

Figure 15. The time history of the primary system with models when $\mu = 0.1$: (a) comparison of this paper and without DVA; (b) comparison between different inerter-to-mass ratios ($\beta = 0.1$ and $\beta = 0.5$).

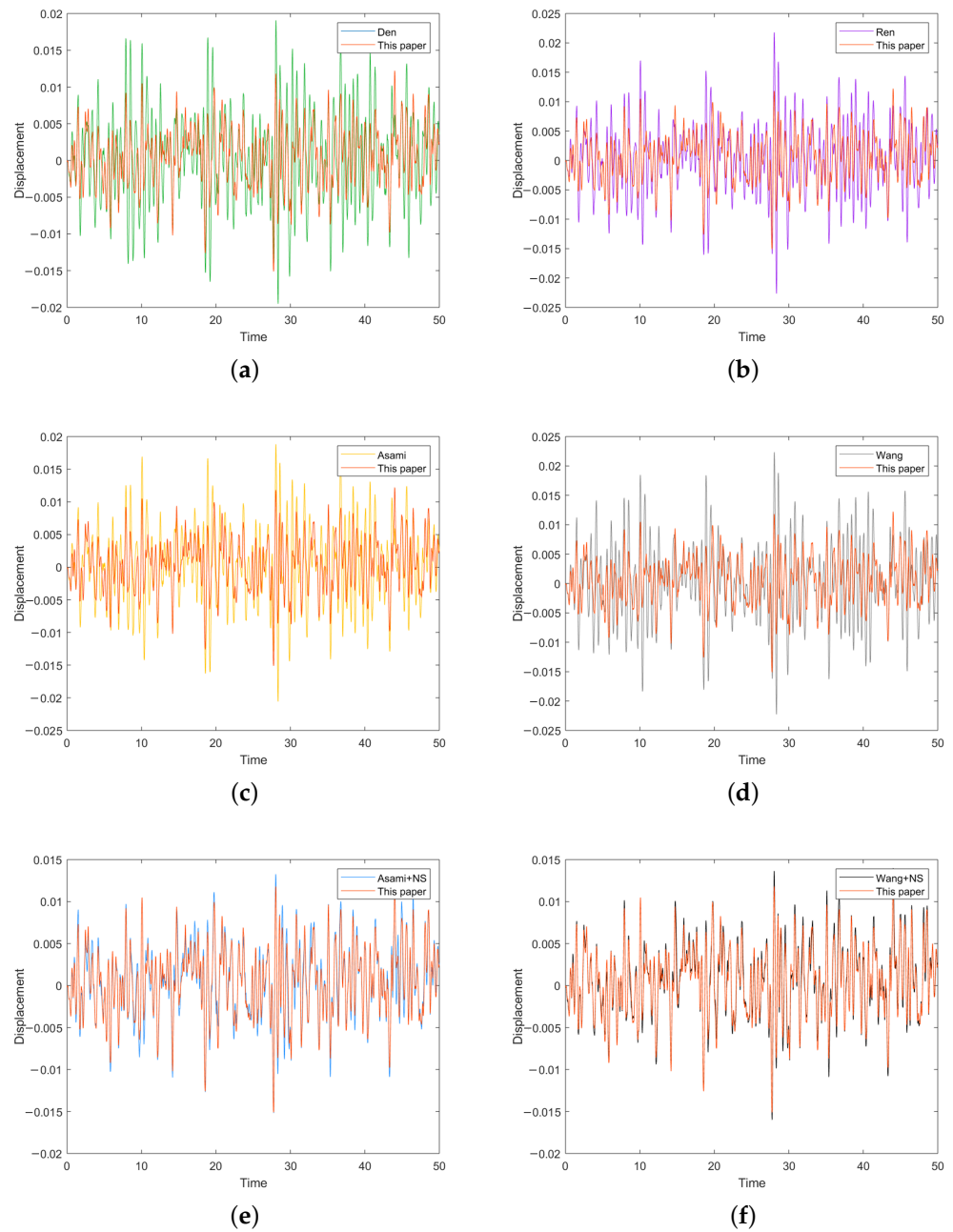


Figure 16. The time history of the primary system with models when $\mu = 0.1$: (a) Den; (b) Ren; (c) Asami; (d) Wang; (e) Asami with negative stiffness; (f) Wang with negative stiffness.

5. Conclusions and Prospects

Vibration phenomena can be found everywhere around us. Vehicles on the ground, aircraft in the air, and ships in the ocean are constantly generating vibration. Many academics concentrate on vibration reduction, vibration isolation, vibration absorption, and other control measures to design and optimize the structure of the vibration source or vibration transmission process because some vibrations may cause wear and consumption of objects. The introduction of DVAs provides an effective path to suppress the vibration of the primary system. The present paper discusses the viscoelastic Maxwell-type DVA model with an inerter and negative stiffness spring under the combination of traditional theory and the intelligent algorithm, which realizes the effect of equal resonance peaks and effectively reduces the amplitude response of the primary system.

On the basis of the H_∞ optimization criterion, the approximate optimal values of frequency ratio, stiffness ratio, and damping ratio are obtained by the fixed-point theory. Using the fourth-order Runge–Kutta method to simulate the analytical solution and the numerical solution, it is found that two peaks of the normalized amplitude–frequency curves are not equal and may be further optimized. Since there are many adjustable parameters in the model, we use the PSO algorithm to observe whether the maximum amplitude of the primary system can be minimized by optimizing the single variable and four variables. After continuously tracking and iterating the individual and global optimal values, the parameters of the final output make the optimized curves achieve equal peaks. For the three cases in which the algorithm is used for optimization in this paper, we obtained our conclusions. From the perspective of amplitude, the amplitude amplification factor gained by optimizing four variable was better than that obtained by optimizing single variables, except for a few cases. From the perspective of the mean square response, it falls between the two cases of optimizing the single variable. In addition, the benefit of all three cases is that the resonance frequency band is widened and the amplitude is suppressed. The analysis of the amplitude–frequency curves, the mean square responses, the variances, and the decreasing ratios of the displacements shows that the presented model is better than other typical DVAs under the optimization of the algorithm. The introduction of the algorithm can not only improve the efficiency of calculating the optimal parameters but also save the calculation time and ensure correctness. The integration of theoretical analysis and intelligent algorithms provides a solid reference for future research of DVAs in parameter optimization and structural design.

Author Contributions: Conceptualization, J.L.; Formal analysis, Y.C.; Funding acquisition, J.L.; Investigation, Y.C.; Methodology, J.L. and Y.C.; Project administration, J.L.; Supervision, J.L.; Validation, S.Z. and Y.C.; Visualization, Y.C. and H.Z.; Writing—original draft, Y.C.; Writing—review and editing, S.Z. and Y.C. All authors contributed equally to this research. All authors have read and agreed to the published version of the manuscript.

Funding: This research is supported by the National Natural Science Foundation of China (Grant No.12272011) and also supported by the National Key R&D Program of China (Grant No. 2022YFB3806000).

Institutional Review Board Statement: Not applicable.

Informed Consent Statement: Not applicable.

Data Availability Statement: The data presented in this study are available on request from the corresponding author.

Acknowledgments: The authors would like to thank all the peer reviewers and editors for their valuable contribution to this work.

Conflicts of Interest: The authors declare no conflict of interest.

Appendix A

Table A1. The specific parameters of the system in different cases of inerter-to-mass ratio when optimizing the single variable ν ($\alpha_{2opt} = \alpha_{2b}$).

Case 1: $\mu = 0.1$								
β	ν_{ori}	$\sigma_{ori}^2(\frac{\pi S_0}{\omega_1^3})$	ν_{opt}	$\sigma_{opt}^2(\frac{\pi S_0}{\omega_1^3})$	A_{max}	λ_{peak1}	λ_{peak2}	$ \lambda_{peak1} - \lambda_{peak2} $
0.1	1.2320	2.7821	1.2617	2.7349	1.8373	0.588	1.230	0.642
0.5	1.3079	2.2072	1.3753	2.1274	1.5504	0.459	1.240	0.781
1.0	1.2516	1.9117	1.3464	1.8151	1.3971	0.368	1.247	0.879
1.5	1.1794	1.7570	1.2903	1.6516	1.3138	0.309	1.253	0.944
2.0	1.1124	1.6612	1.2333	1.5503	1.2607	0.268	1.258	0.990

Table A1. Cont.

Case 2: $\mu = 0.2$								
β	ν_{ori}	$\sigma_{ori}^2(\frac{\pi S_0}{\omega_1^3})$	ν_{opt}	$\sigma_{opt}^2(\frac{\pi S_0}{\omega_1^3})$	A_{max}	λ_{peak1}	λ_{peak2}	$ \lambda_{peak1} - \lambda_{peak2} $
0.1	0.9063	2.5747	0.9354	2.5158	1.7348	0.547	1.234	0.687
0.5	0.9200	2.1280	0.9724	2.0436	1.5099	0.436	1.242	0.806
1.0	0.8749	1.8735	0.9446	1.7748	1.3768	0.354	1.249	0.895
1.5	0.8241	1.7344	0.9041	1.6278	1.3014	0.300	1.254	0.954
2.0	0.7778	1.6463	0.8644	1.5344	1.2523	0.261	1.259	0.998
Case 3: $\mu = 0.3$								
β	ν_{ori}	$\sigma_{ori}^2(\frac{\pi S_0}{\omega_1^3})$	ν_{opt}	$\sigma_{opt}^2(\frac{\pi S_0}{\omega_1^3})$	A_{max}	λ_{peak1}	λ_{peak2}	$ \lambda_{peak1} - \lambda_{peak2} $
0.1	0.7523	2.4220	0.7818	2.3543	1.6587	0.513	1.236	0.723
0.5	0.7454	2.0613	0.7917	1.9732	1.4755	0.416	1.243	0.827
1.0	0.7059	1.8396	0.7649	1.7390	1.3586	0.341	1.250	0.909
1.5	0.6649	1.7138	0.7316	1.6059	1.2900	0.291	1.255	0.964
2.0	0.6281	1.6324	0.6996	1.5196	1.2445	0.255	1.259	1.004
Case 4: $\mu = 0.4$								
β	ν_{ori}	$\sigma_{ori}^2(\frac{\pi S_0}{\omega_1^3})$	ν_{opt}	$\sigma_{opt}^2(\frac{\pi S_0}{\omega_1^3})$	A_{max}	λ_{peak1}	λ_{peak2}	$ \lambda_{peak1} - \lambda_{peak2} $
0.1	0.6548	2.3031	0.6847	2.2286	1.5990	0.484	1.238	0.754
0.5	0.6395	2.0043	0.6823	1.9129	1.4458	0.399	1.245	0.846
1.0	0.6040	1.8092	0.6567	1.7068	1.3422	0.330	1.251	0.921
1.5	0.5691	1.6948	0.6279	1.5858	1.2795	0.283	1.256	0.973
2.0	0.5380	1.6194	0.6006	1.5059	1.2371	0.248	1.260	1.012

Table A2. Symbols and nomenclature.

m_1	mass of the primary system	m_2	mass of the absorber system
k_1	stiffness of the primary system	k_2	stiffness of the absorber system
k_3	stiffness of the Maxwell structure	k_4	negative stiffness of the grounded spring
c	damping of the Maxwell structure	b	inserter
F_0	amplitude of the force excitation	ω	frequency of the force excitation
ζ	damping ratio ($\zeta = \frac{c}{2m_2\omega_2}$)	μ	mass ratio ($\mu = \frac{m_2}{m_1}$)
α_1	ratio of spring constants ($\alpha_1 = \frac{k_3}{k_1}$)	α_2	ratio of spring constants ($\alpha_2 = \frac{k_4}{k_1}$)
β	inserter-to-mass ratio ($\beta = \frac{b}{m_1}$)	f	amplitude-to-mass ratio ($f = \frac{F_0}{m_1}$)
ν	natural frequency ratio ($\nu = \frac{\omega_2}{\omega_1}$)	λ	forced frequency ratio ($\lambda = \frac{\omega}{\omega_1}$)
x_1	displacement of the primary system	x_2	displacement of the absorber system
x_3	displacement of the division point about spring and damping in Maxwell structure		
ω_1	natural frequency of the primary system ($\omega_1 = \sqrt{\frac{k_1}{m_1}}$)		
ω_2	natural frequency of the absorber system ($\omega_2 = \sqrt{\frac{k_2}{m_2}}$)		
X_{st}	static deformation of the primary system ($X_{st} = \frac{F_0}{k_1}$)		
A	amplitude amplification factor of the primary system		
σ^2	mean square response of the primary system		

References

- Ormondroyd, J.; Den Hartog, J.P. The theory of the dynamic vibration absorber. *ASME J. Appl. Mech.* **1928**, *50*, 9–22.
- Hahnkamm, E. The damping of the foundation vibrations at varying excitation frequency. *Master Archit.* **1932**, *4*, 192–201.
- Brock, J.E. A note on the damped vibration absorber. *ASME J. Appl. Mech.* **1946**, *13*, A284. [[CrossRef](#)]

4. Den Hartog, J.P. *Mechanical Vibrations*; McGraw-Hill Book Company: New York, NY, USA, 1947.
5. Asami, T.; Nishihara, O. Analytical and experimental evaluation of an air damped dynamic vibration absorber: Design optimizations of the three-element type model. *J. Vib. Acoust.* **1999**, *121*, 334–342. [[CrossRef](#)]
6. Ren, M.Z. A variant design of the dynamic vibration absorber. *J. Sound Vib.* **2001**, *245*, 762–770. [[CrossRef](#)]
7. Asami, T.; Sekiguchi, H. Fundamental investigation on air damper (1st report, theoretical analysis). *Trans. Jpn. Soc. Mech. Eng.* **1990**, *56*, 1400–1407. (In Japanese) [[CrossRef](#)]
8. Asami, T.; Sekiguchi, H. Fundamental investigation on air damper (2nd report, theoretical and experimental study). *Trans. Jpn. Soc. Mech. Eng.* **1990**, *56*, 3201–3209. (In Japanese) [[CrossRef](#)]
9. Asami, T.; Nishihara, O.; Baz, A.M. Analytical solutions to H_∞ and H_2 optimization of dynamic vibration absorbers attached to damped linear systems. *J. Vib. Acoust.* **2002**, *124*, 284–295. [[CrossRef](#)]
10. Asami, T.; Nishihara, O. H_2 optimization of the three-element type dynamic vibration absorbers. *J. Vib. Acoust.* **2002**, *124*, 583–592. [[CrossRef](#)]
11. Nishihara, O.; Asami, T. Closed-form solutions to the exact optimizations of dynamic vibration absorbers (minimizations of the maximum amplitude magnification factors). *J. Vib. Acoust.* **2002**, *124*, 576–582. [[CrossRef](#)]
12. Asami, T.; Nishihara, O. Closed-form exact solution to H_∞ optimization of dynamic vibration absorbers (application to different transfer functions and damping systems). *J. Vib. Acoust.* **2003**, *125*, 398–405. [[CrossRef](#)]
13. Lakes, R.S.; Lee, T.; Bersie, A.; Wang, Y.C. Extreme damping in composite materials with negative-stiffness inclusions. *Nature* **2001**, *410*, 565–567. [[CrossRef](#)] [[PubMed](#)]
14. Lakes, R.S.; Drugan, W.J. Dramatically stiffer elastic composite materials due to a negative stiffness phase? *J. Mech. Phys. Solids* **2002**, *50*, 979–1009. [[CrossRef](#)]
15. Wu, L.T.; Wang, K. Optimization design and stability analysis for a new class of inerter-based dynamic vibration absorbers with a spring of negative stiffness. *J. Vib. Control* **2022**, *0*, 1–15. [[CrossRef](#)]
16. Mantakas, A.G.; Kapasakalis, K.A.; Alvertos, A.E.; Antoniadis, I.A.; Sapountzakis, E.J. A negative stiffness dynamic base absorber for seismic retrofitting of residential buildings. *Struct. Control Health Monit.* **2022**, *29*, e3127. [[CrossRef](#)]
17. Shen, Y.J.; Wang, X.R.; Yang, S.P.; Xing, H.J. Parameters optimization for a kind of dynamic vibration absorber with negative stiffness. *Math. Probl. Eng.* **2016**, *2016*, 9624325. [[CrossRef](#)]
18. Shen, Y.J.; Peng, H.B.; Li, X.H.; Yang, S.P. Analytically optimal parameters of dynamic vibration absorber with negative stiffness. *Mech. Syst. Signal Pr.* **2017**, *85*, 193–203. [[CrossRef](#)]
19. Smith, M.C. Synthesis of mechanical networks: The inerter. *IEEE Trans. Automat. Contr.* **2002**, *47*, 1648–1662. [[CrossRef](#)]
20. Wang, F.C.; Liao, M.K.; Liao, B.H.; Su, W.J.; Chan, H.A. The performance improvements of train suspension systems with mechanical networks employing inerters. *Veh. Syst. Dyn.* **2009**, *47*, 805–830. [[CrossRef](#)]
21. Chen, M.Z.Q.; Hu, Y.L.; Huang, L.X.; Chen, G.R. Influence of inerter on natural frequencies of vibration systems. *J. Sound Vib.* **2014**, *333*, 1874–1887. [[CrossRef](#)]
22. Barredo, E.; Blanco, A.; Colin, J.; Penagos, V.M.; Abundez, A.; Vela, L.G.; Meza, V.; Cruz, R.H.; Mayen, J. Closed-form solutions for the optimal design of inerter-based dynamic vibration absorbers. *Int. J. Mech. Sci.* **2018**, *144*, 41–53. [[CrossRef](#)]
23. Barredo, E.; Larios, J.G.M.; Colin, J.; Mayen, J.; Flores-Hernandez, A.A.; Arias-Montiel, M. A novel high-performance passive non-traditional inerter-based dynamic vibration absorber. *J. Sound Vib.* **2020**, *485*, 115583. [[CrossRef](#)]
24. Wang, X.R.; Liu, X.D.; Shan, Y.C.; Shen, Y.J.; He, T. Analysis and optimization of the novel inerter-based dynamic vibration absorbers. *IEEE Access* **2018**, *6*, 33169–33182. [[CrossRef](#)]
25. Wang, X.R.; He, T.; Shen, Y.J.; Shan, Y.C.; Liu, X.D. Parameters optimization and performance evaluation for the novel inerter-based dynamic vibration absorbers with negative stiffness. *J. Sound Vib.* **2019**, *463*, 114941. [[CrossRef](#)]
26. Shen, Y.J.; Xing, Z.Y.; Yang, S.P.; Sun, J.Q. Parameters optimization for a novel dynamic vibration absorber. *Mech. Syst. Signal Pr.* **2019**, *133*, 106282. [[CrossRef](#)]
27. Zhu, X.Z.; Chen, Z.B.; Jiao, Y.H. Optimizations of distributed dynamic vibration absorbers for suppressing vibrations in plates. *J. Low Freq. Noise Vib. Act. Control* **2018**, *37*, 1188–1200. [[CrossRef](#)]
28. Basta, E.; Ghommam, M.; Emam, S. Flutter control and mitigation of limit cycle oscillations in aircraft wings using distributed vibration absorbers. *Nonlinear Dyn.* **2021**, *106*, 1975–2003. [[CrossRef](#)]
29. Zhang, M.J.; Xu, F.Y. Tuned mass damper for self-excited vibration control: Optimization involving nonlinear aeroelastic effect. *J. Wind. Eng. Ind. Aerodyn.* **2022**, *220*, 104836. [[CrossRef](#)]
30. Wang, Q.; Zhou J.X.; Wang, K.; Gao, J.H.; Lin, Q.D.; Chang, Y.P.; Xu, D.L.; Wen, G.L. Dual-function quasi-zero-stiffness dynamic vibration absorber: Low-frequency vibration mitigation and energy harvesting. *Appl. Math. Model.* **2023**, *116*, 636–654. [[CrossRef](#)]
31. Gad, A.G. Particle swarm optimization algorithm and its applications: A systematic review. *Arch. Comput. Methods Eng.* **2022**, *29*, 2531–2561. [[CrossRef](#)]
32. Jain, M.; Saihjjal, V.; Singh, N.; Singh, S.B. An overview of variants and advancements of PSO algorithm. *Appl. Sci.* **2022**, *12*, 8392. [[CrossRef](#)]

33. Wang, X.R.; Shen, Y.J.; Yang, S.P. H_∞ optimization of the grounded three-element type dynamic vibration absorber. *J. Dyn. Contr.* **2016**, *14*, 448–453. (In Chinese)
34. Wang, X.R.; Shen, Y.J.; Yang, S.P.; Xing, H.J. H_∞ parameter optimization of three-element type dynamic vibration absorber with negative stiffness. *J. Vib. Eng.* **2017**, *30*, 177–184. (In Chinese)

Disclaimer/Publisher's Note: The statements, opinions and data contained in all publications are solely those of the individual author(s) and contributor(s) and not of MDPI and/or the editor(s). MDPI and/or the editor(s) disclaim responsibility for any injury to people or property resulting from any ideas, methods, instructions or products referred to in the content.